Variational Multiscale Analysis: the Fine-scale Green's Function, Projection, Optimization, Localization, and Stabilized Methods

T.J.R. Hughes* and G. Sangalli♮

*The University of Texas at Austin
Institute for Computational Engineering and Sciences
1 University Station C0200
Austin, TX 78712-0027, U.S.A.

♮ Istituto di Matematica Applicata e Tecnologie Informatiche
Consiglio Nazionale delle Ricerche
Via Ferrata, 1
27100 Pavia, Italy

Abstract

We derive an explicit formula for the fine-scale Green's function arising in variational multiscale analysis. The formula is expressed in terms of the classical Green's function and a projector which defines the decomposition of the solution into coarse and fine scales. The theory is presented in an abstract operator format and subsequently specialized for the advection-diffusion equation. It is shown that different projectors lead to fine-scale Green's functions with very different properties. For example, in the advection-dominated case, the projector induced by the H_0^1-seminorm produces a fine-scale Green's function which is highly attenuated and localized. These are very desirable properties in a multiscale method, and ones that are not shared by the L^2-projector. By design, the coarse-scale solution attains optimality in the norm associated with the projector. This property, combined with a localized fine-scale Green's function, indicates the possibility of effective methods with local character for dominantly hyperbolic problems. The constructs lead to a new class of stabilized methods, and the relationship between H_0^1-optimality and SUPG is described.

Contents

1 Introduction

The variational multiscale method [13, 14] was introduced as a framework for incorporating missing fine-scale effects into numerical problems governing coarse-scale behavior. It has provided a rationale for stabilized methods, and a platform for the development of new methods (see, e.g., [11, 12, 15–17] for application to turbulence modeling). The fundamental mathematical object in the method is the so-called *fine-scale Green's function*, introduced in [14]. Although it is a simple matter to characterize coarse-scale and fine-scale subspaces, not much is known about the fine-scale Green's function. In this paper, we study the fine-scale Green's function and present a formula for explicitly computing it from the classical Green's function. This is accomplished by observing that the decomposition of a function into a sum of coarse-scale and fine-scale components is uniquely specified by identifying a projector from the space of all scales onto the coarse-scale subspace. Different projectors produce different decompositions. The problem for the fine-scale Green's function is then posed in terms of the fine-scale subspace. Compared with the problem for the classical Green's function, this amounts to a constrained formulation. The constraint can be released by invoking the Lagrange multiplier method and the unconstrained problem can be solved in terms of the classical Green's function and the projector. The fine-scale Green's function enjoys orthogonality relations with respect to the projector. If a scalar product is introduced with corresponding projector, the coarse-scale solution of the original problem is the optimal approximation in terms of the induced norm. The theory summarizing these ideas is presented in Section 2 in an abstract operator format for a general linear isomorphism.

These ideas are applied to the advection-diffusion equation in Section 3. The fine-scale Green's function is explicitly calculated in one dimension for linear, quadratic, and cubic finite elements when the projector is defined by the H_0^1-seminorm. In this case, the fine-scale Green's function is local in that it is confined to individual elements and is not coupled from one element to another, even in advection-dominated cases. This is a highly-desirable property in multiscale analysis and in complete contrast with the classical Green's function which exhibits global support in advection-dominated cases. It also suggests that efficient, approximate, multiscale methods possessing local character may be possible for dominantly hyperbolic phenomena. On the other hand, selecting

the L^2-projector results in a fine-scale Green's function with global coupling. These results show clearly that the choice of projector is of key importance in the development of a multiscale method.

The fine-scale Green's functions become increasingly complicated as the order of the coarse-scale space is increased. However, it is observed that due to the orthogonality properties of the fine-scale Green's function, it only interacts with the highest-order polynomial term in the residual. This means that for a kth-order coarse-scale space, the fine-space Green's function modification to the coarse-scale equation can be replaced by an equivalent stabilization term involving a computable, elements-wise constant (i.e., a "τ" in the notation of stabilized methods), and derivatives of the residual and weighting operator of order $k-1$. Remarkably, the modification reduces to element-wise constant terms requiring no quadrature despite the complexity of the fine-scale Green's function.

To assess the situation in multiple dimensions, the two-dimensional advection-diffusion equation is studied. Here, rather than proceeding analytically, numerical procedures involving very fine meshes are utilized to determine Green's functions. As in the one-dimensional case, the classical Green's function exhibits global character with support in the form of a tail surrounding the upwind characteristic through the point of application of the Dirac mass. When advection-dominated, this tail is not attenuated with distance. However, the fine-scale Green's function for the H^1_0-projector is highly attenuated under the same circumstances and is essentially confined to a small number of elements (in the coarse-scale space) surrounding the point of application of the Dirac mass. The L^2-projector engenders a fine-scale Green's function which is not localized and one concludes that the main observations made for the one-dimensional case are essentially true in two dimensions.

The H^1_0-projector produces a method which is highly localized and attains an optimal approximation in the H^1_0-seminorm, a combination of desirable properties. It is also noted that the modification it introduces to a classical Galerkin formulation involves an additional stabilization term in which the coarse-scale residual is weighted by the fine-scale Green's function convolved only with the advective part of the operator, that is, the diffusive operator does not appear in the weighting. These are features that the H^1_0-optimal method has in common with SUPG [9].

In Section 4 we draw conclusions.

2 The abstract framework

2.1 The abstract problem

Let V be a Hilbert space, endowed with a norm $\|\cdot\|_V$ and a scalar product $(\cdot,\cdot)_V$. Let V^* be the dual of V and let ${}_{V^*}\langle\cdot,\cdot\rangle_V$ be the pairing between them. Let $\mathcal{L}: V \to V^*$ be a linear isomorphism. Given $f \in V^*$, we consider the abstract problem of finding $u \in V$ such that

$$\mathcal{L}u = f. \tag{1}$$

The variational formulation of (1) is: find $u \in V$ such that

$${}_{V^*}\langle \mathcal{L}u, v\rangle_V = {}_{V^*}\langle f, v\rangle_V, \qquad \forall v \in V. \tag{2}$$

The solution u can be expressed as $u = \mathcal{G}f$, where $\mathcal{G}: V^* \to V$ is the Green's operator, that is $\mathcal{G} = \mathcal{L}^{-1}$.

2.2 The variational multiscale formulation

Let $\bar{V}$ be a closed subspace of V, and let $\mathcal{P}$ be a linear projector onto $\bar{V}$, that is, $\mathcal{P}^2 = \mathcal{P}$ and $\text{Range}(\mathcal{P}) = \bar{V}$. We assume $\mathcal{P}$ to be continuous in V. We also have the obvious inf-sup condition

$$\inf_{\bar{v}\in\bar{V}} \sup_{w\in V} \frac{(\mathcal{P}w, \bar{v})_V}{\|w\|_V \|\bar{v}\|_V} \geq 1. \tag{3}$$

We define $V' = \text{Ker}(\mathcal{P})$, which is also a closed subspace of V. In the variational multiscale (VMS) approach, $\bar{V}$ represents the space of computable *coarse scales*, while V' contains the unresolved *fine scales*. Notice that

$$V = \bar{V} \oplus V', \tag{4}$$

that is, any $v \in V$ can be written uniquely as $v = \bar{v} + v'$, where $\bar{v} \in \bar{V}$ and $v' \in V'$: indeed, $\bar{v} = \mathcal{P}v$ and $v' = v - \mathcal{P}v$. In particular, we split the solution u of (1) as $u = \bar{u} + u'$. The aim of the VMS approach is to obtain $\bar{u} = \mathcal{P}u$.

The variational formulation (2) splits into

$$ {}_{V^*}\langle \mathcal{L}\bar{u}, \bar{v}\rangle_V + {}_{V^*}\langle \mathcal{L}u', \bar{v}\rangle_V = {}_{V^*}\langle f, \bar{v}\rangle_V, \qquad \forall \bar{v} \in \bar{V}, \tag{5}$$

$$ {}_{V^*}\langle \mathcal{L}\bar{u}, v'\rangle_V + {}_{V^*}\langle \mathcal{L}u', v'\rangle_V = {}_{V^*}\langle f, v'\rangle_V, \qquad \forall v' \in V'. \tag{6}$$

We assume that (5) is a well-posed problem for $\bar{u}$ alone, meaning that it admits a unique solution $\bar{u} \in \bar{V}$, given u' and f. Analogously, we assume that (6) is well-posed for $u' \in V'$, given $\bar{u}$ and f. For that, we ask the inf-sup conditions for $\mathcal{L}$ on $\bar{V}$ and V'

$$\inf_{\bar{w}\in\bar{V}} \sup_{\bar{v}\in\bar{V}} \frac{{}_{V^*}\langle \mathcal{L}\bar{w}, \bar{v}\rangle_V}{\|\bar{w}\|_V \|\bar{v}\|_V} > 0 \qquad \text{and} \qquad \sup_{\bar{w}\in\bar{V}} \frac{{}_{V^*}\langle \mathcal{L}\bar{w}, \bar{v}\rangle_V}{\|\bar{w}\|_V} > 0, \quad \forall \bar{v} \in \bar{V}, \bar{v} \neq 0, \tag{7}$$

$$\inf_{w'\in V'} \sup_{v'\in V'} \frac{{}_{V^*}\langle \mathcal{L}w', v'\rangle_V}{\|w'\|_V \|v'\|_V} > 0 \qquad \text{and} \qquad \sup_{w'\in V'} \frac{{}_{V^*}\langle \mathcal{L}w', v'\rangle_V}{\|w'\|_V} > 0, \quad \forall v' \in V', v' \neq 0. \tag{8}$$

If $\mathcal{L}$ is coercive on V, that is, ${}_{V^*}\langle \mathcal{L}v, v\rangle_V \geq C\|v\|_V^2$ for $C > 0$ and for all $v \in V$, then (7)–(8) hold.

We associate with (6) the *fine-scale Green's operator* $\mathcal{G}' : V^* \to V'$, which gives u' from the coarse-scale *residual* $f - \mathcal{L}\bar{u}$, that is,

$$u' = \mathcal{G}'(f - \mathcal{L}\bar{u}). \tag{9}$$

Having $\mathcal{G}'$, we can eliminate u' from (5), and we obtain the VMS formulation for $\bar{u}$:

$$ {}_{V^*}\langle \mathcal{L}\bar{u}, \bar{v}\rangle_V - {}_{V^*}\langle \mathcal{L}\mathcal{G}'\mathcal{L}\bar{u}, \bar{v}\rangle_V = {}_{V^*}\langle f, \bar{v}\rangle_V - {}_{V^*}\langle \mathcal{L}\mathcal{G}'f, \bar{v}\rangle_V, \qquad \forall \bar{v} \in \bar{V}. \tag{10}$$

Because of (4), the formulation (10) admits a unique solution, which is precisely $\bar{u} = \mathcal{P}u$.

2.3 The fine-scale Green's operator

We denote by $\mathcal{P}^T : \bar{V}^* \to V^*$ the transpose of $\mathcal{P}$, that is

$$ {}_{V^*}\langle \mathcal{P}^T\bar{\mu}, v\rangle_V = {}_{\bar{V}^*}\langle \bar{\mu}, \mathcal{P}v\rangle_{\bar{V}}, \qquad \forall v \in V, \bar{\mu} \in \bar{V}^*,$$

where $\bar{V}^*$ is the dual of $\bar{V}$, and ${}_{\bar{V}^*}\langle \cdot, \cdot\rangle_{\bar{V}}$ is the pairing between them.

In the next result we express $\mathcal{G}'$ in terms of $\mathcal{G}$ and $\mathcal{P}$.

Theorem 1. *Under the assumptions of Sections 2.1–2.2, we have*

$$\mathcal{G}' = \mathcal{G} - \mathcal{G}\mathcal{P}^T(\mathcal{P}\mathcal{G}\mathcal{P}^T)^{-1}\mathcal{P}\mathcal{G}. \tag{11}$$

Furthermore,

$$\mathcal{G}'\mathcal{P}^T = 0, \tag{12}$$
$$\mathcal{P}\mathcal{G}' = 0. \tag{13}$$

Proof. Since (6) is a constrained problem, we can rephrase it making use of a Lagrange multiplier in mixed (unconstrained) form: find $u' \in V$, and $\bar{\lambda} \in \bar{V}^*$ such that

$$\mathcal{L}u' + \mathcal{P}^T\bar{\lambda} = r, \tag{14}$$
$$\mathcal{P}u' = 0, \tag{15}$$

where $r = f - \mathcal{L}\bar{u}$. The well-posedness of (14)–(15), for any $r \in V^*$, is guaranteed by our previous assumptions (3) and (8) (see [2]). From (14) we get

$$u' = \mathcal{G}(r - \mathcal{P}^T\bar{\lambda}); \tag{16}$$

substituting in (15) gives

$$\mathcal{P}\mathcal{G}r - \mathcal{P}\mathcal{G}\mathcal{P}^T\bar{\lambda} = 0;$$

the well-posedness of (14)–(15) guarantees the invertibility of $\mathcal{P}\mathcal{G}\mathcal{P}^T$, hence we obtain

$$\bar{\lambda} = (\mathcal{P}\mathcal{G}\mathcal{P}^T)^{-1}\mathcal{P}\mathcal{G}r.$$

Finally, using this in (16) yields

$$u' = (\mathcal{G} - \mathcal{G}\mathcal{P}^T(\mathcal{P}\mathcal{G}\mathcal{P}^T)^{-1}\mathcal{P}\mathcal{G})r, \tag{17}$$

which gives (11).

From (11), we immediately have

$$\mathcal{G}'\mathcal{P}^T = \mathcal{G}\mathcal{P}^T - \mathcal{G}\mathcal{P}^T(\mathcal{P}\mathcal{G}\mathcal{P}^T)^{-1}(\mathcal{P}\mathcal{G}\mathcal{P}^T) = \mathcal{G}\mathcal{P}^T - \mathcal{G}\mathcal{P}^T = 0,$$

and

$$\mathcal{P}\mathcal{G}' = \mathcal{P}\mathcal{G} - (\mathcal{P}\mathcal{G}\mathcal{P}^T)(\mathcal{P}\mathcal{G}\mathcal{P}^T)^{-1}\mathcal{P}\mathcal{G} = \mathcal{P}\mathcal{G} - \mathcal{P}\mathcal{G} = 0.$$

□

Using the expression (11), in (10), we see that the left-hand side of (10) is

$${}_{V^*}\langle \mathcal{L}\bar{u}, \bar{v}\rangle_V - {}_{V^*}\langle \mathcal{L}\mathcal{G}'\mathcal{L}\bar{u}, \bar{v}\rangle_V = {}_{\bar{V}^*}\langle (\mathcal{P}\mathcal{G}\mathcal{P}^T)^{-1}\bar{u}, \bar{v}\rangle_{\bar{V}}\,. \tag{18}$$

As $(\mathcal{P}\mathcal{G}\mathcal{P}^T)^{-1}$ is obviously invertible, (18) confirms that (10) is a well-posed formulation.

In the cases of practical interest, $\bar{V}$ is a finite-dimensional subspace of V. If the dimension of $\bar{V}$ is N, then we can find a set of functionals $\{\mu_i\}_{i=1,\dots,N}$ such that for all $v \in V$

$${}_{V^*}\langle \mu_i, v\rangle_V = 0, \quad \forall i = 1, \dots, N \qquad \Leftrightarrow \qquad \mathcal{P}v = 0. \tag{19}$$

In other words, the equations ${}_{V^*}\langle \mu_i, v\rangle_V = 0$, for $1 \le i \le N$, characterize v as a fine-scale function, that is $v \in V'$. From the mathematical standpoint, $\{\mu_i\}_{i=1,\dots,N}$ is a basis for the image of $\mathcal{P}^T$. Therefore, it is clear that (12) and (13) are equivalent to

$$ {}_{V^*}\langle \mu_i, \mathcal{G}'\nu\rangle_V = 0, \qquad \forall \nu \in V^*, \forall i = 1, \dots, N, \tag{20}$$

and

$$ \mathcal{G}'\mu_i = 0, \qquad \forall i = 1, \dots, N. \tag{21}$$

Moreover, after introducing the vector $\boldsymbol{\mu} \in (V^*)^N$ and its transpose

$$ \boldsymbol{\mu} = \begin{bmatrix} \mu_1 \\ \vdots \\ \mu_N \end{bmatrix} \qquad \text{and} \qquad \boldsymbol{\mu}^T = \begin{bmatrix} \mu_1 & \dots & \mu_N \end{bmatrix}, $$

the vector $\mathcal{G}\boldsymbol{\mu}^T \in V^N$

$$ \mathcal{G}\boldsymbol{\mu}^T = \begin{bmatrix} \mathcal{G}\mu_1 & \dots & \mathcal{G}\mu_N \end{bmatrix}, $$

the matrix $\boldsymbol{\mu}\mathcal{G}\boldsymbol{\mu}^T \in \mathbb{R}^{N\times N}$

$$ \boldsymbol{\mu}\mathcal{G}\boldsymbol{\mu}^T = \begin{bmatrix} {}_{V^*}\langle \mu_1, \mathcal{G}\mu_1\rangle_V & \dots & {}_{V^*}\langle \mu_1, \mathcal{G}\mu_N\rangle_V \\ \vdots & \ddots & \vdots \\ {}_{V^*}\langle \mu_N, \mathcal{G}\mu_1\rangle_V & \dots & {}_{V^*}\langle \mu_N, \mathcal{G}\mu_N\rangle_V \end{bmatrix}, $$

and the vector of functionals $\boldsymbol{\mu}\mathcal{G} : (V^*) \to \mathbb{R}^N$ (i.e., $\boldsymbol{\mu}\mathcal{G} \in (V^{**})^N$) such that

$$ \boldsymbol{\mu}\mathcal{G}(\nu) = \begin{bmatrix} {}_{V^*}\langle \mu_1, \mathcal{G}\nu\rangle_V \\ \vdots \\ {}_{V^*}\langle \mu_N, \mathcal{G}\nu\rangle_V \end{bmatrix}, \quad \forall \nu \in V^*, $$

it is easy to see that (11) is equivalent to

$$ \mathcal{G}' = \mathcal{G} - \mathcal{G}\boldsymbol{\mu}^T \left[\boldsymbol{\mu}\mathcal{G}\boldsymbol{\mu}^T\right]^{-1} \boldsymbol{\mu}\mathcal{G}. \tag{22}$$

2.4 Orthogonal projectors and optimization

An interesting case, and the only one considered in what follows, is when $\mathcal{P}$ is an orthogonal projector.

Given a scalar product $(\cdot,\cdot)$ defined on $V \times V$, possibly different than $(\cdot,\cdot)_V$, the related orthogonal projector $\mathcal{P}$ is obviously defined by

$$ (\mathcal{P}w, \bar{v}) = (w, \bar{v}), \qquad \forall w \in V, \forall \bar{v} \in \bar{V}. \tag{23}$$

Recall that, in order to fit in the abstract framework of Section 2.2, $\mathcal{P}$ must be a continuous operator in V. However, when $\bar{V}$ is a finite-dimensional space, this holds for any scalar product $(\cdot,\cdot)$ which is continuous on $V \times V$.

In this context, the VMS formulation provides the optimal approximation $\bar{u} \in \bar{V}$ of u, with respect to the norm $\|\cdot\|$ induced by the scalar product $(\cdot,\cdot)$.

3 The advection-diffusion model problem

Let d be the space dimension ($d = 1$ and $d = 2$ will be taken into consideration in the examples) and let $\Omega \subset \mathbb{R}^d$ be a regular domain. We consider the advection-diffusion model problem

$$\mathcal{L}u = -\kappa\Delta u + \beta \cdot \nabla u = f \text{ in } \Omega, \qquad \text{with } u_{|\partial\Omega} = 0, \tag{24}$$

where $f \in L^2(\Omega)$ is the source term, $\kappa > 0$ is the scalar diffusivity and $\beta : \Omega \to \mathbb{R}^d$ is the advection velocity, for which we assume $\mathrm{div}(\beta) = 0$. For the variational formulation of (24), within the framework of Section 2, we set $V = H^1_0 \equiv H^1_0(\Omega)$, whence $V^* = H^{-1}$. Typical finite element spaces will be considered as coarse spaces $\bar{V}$.

In this context, it is convenient to represent the Green's operator $\mathcal{G}$ through the Green's function $g : \Omega \times \Omega \to \mathbb{R}$ such that

$$u(y) = \int_\Omega g(x, y) f(x)\, dx. \tag{25}$$

We have $g_{|\partial(\Omega\times\Omega)} = 0$ and, for all $y \in \Omega$, $\mathcal{L}^* g(\cdot, y) = \delta(\cdot - y)$, where δ is the Dirac mass at the origin and $\mathcal{L}^* = -\kappa\Delta - \beta \cdot \nabla$ denotes the dual of $\mathcal{L}$. Indeed

$$u(y) = \int_\Omega \delta(x - y)u(x)\, dx = \int_\Omega \mathcal{L}^* g(x, y)u(x)\, dx = \int_\Omega g(x, y)\mathcal{L}u(x)\, dx = \int_\Omega g(x, y)f(x)\, dx.$$

We also recall that $\mathcal{L}^* g(\cdot, y) = \mathcal{L}g(y, \cdot)$.

Furthermore, we introduce the fine-scale Green's function $g' : \Omega \times \Omega \to \mathbb{R}$, which represents the fine-scale Green's operator $\mathcal{G}'$ and gives the fine-scale component u' of u from the coarse-scale residual $r = f - \mathcal{L}\bar{u}$ by

$$u'(y) = \int_\Omega g'(x, y)r(x)\, dx. \tag{26}$$

Recall, however, that the space of fine scales V' as well as the fine-scale Green's function g' depend on the coarse-scale space $\bar{V}$ and the underlying projector $\mathcal{P}$. With an abuse of notation, in the next sections we shall write V' and g' without distinction among the different coarse spaces and projectors taken into consideration. In particular, we will deal with the H^1_0-projector $\mathcal{P} = \mathcal{P}_{H^1_0}$, associated with the scalar product

$$(w, v) = (w, v)_{H^1_0} = \int_\Omega \nabla w(x) \cdot \nabla v(x)\, dx,$$

and the usual L^2-projector $\mathcal{P} = \mathcal{P}_{L^2}$. Having a set of functionals $\{\mu_i\}_{i=1,\dots,N}$ as in (19), that is, giving

$$\int_\Omega \mu_i(x)v(x)\, dx = 0, \quad \forall i = 1, \dots, N \qquad \Leftrightarrow \qquad \mathcal{P}v = 0, \tag{27}$$

then g' is obtained straightforwardly by (22) as

$$\begin{aligned} g'(x, y) = g(x, y) &- \begin{bmatrix} \int_\Omega g(\tilde{x}, y)\mu_1(\tilde{x})\, d\tilde{x} & \dots & \int_\Omega g(\tilde{x}, y)\mu_N(\tilde{x})\, d\tilde{x} \end{bmatrix} \\ &\times \begin{bmatrix} \int_\Omega g(\tilde{x}, \tilde{y})\mu_1(\tilde{x})\mu_1(\tilde{y})\, d\tilde{x}d\tilde{y} & \dots & \int_\Omega g(\tilde{x}, \tilde{y})\mu_N(\tilde{x})\mu_1(\tilde{y})\, d\tilde{x}d\tilde{y} \\ \vdots & \ddots & \vdots \\ \int_\Omega g(\tilde{x}, \tilde{y})\mu_1(\tilde{x})\mu_N(\tilde{y})\, d\tilde{x}d\tilde{y} & \dots & \int_\Omega g(\tilde{x}, \tilde{y})\mu_N(\tilde{x})\mu_N(\tilde{y})\, d\tilde{x}d\tilde{y} \end{bmatrix}^{-1} \\ &\times \begin{bmatrix} \int_\Omega g(x, \tilde{y})\mu_1(\tilde{y})\, d\tilde{y} \\ \vdots \\ \int_\Omega g(x, \tilde{y})\mu_N(\tilde{y})\, d\tilde{y} \end{bmatrix}, \end{aligned} \tag{28}$$

while (20) and (21) mean

$$\int_\Omega g'(\tilde{x},y)\mu_i(\tilde{x})\,d\tilde{x}=0,\ \text{and}\ \int_\Omega g'(x,\tilde{y})\mu_i(\tilde{y})\,d\tilde{y}=0,\qquad \forall x,y\in\Omega,\forall i=1,\dots,N. \tag{29}$$

In this context, the VMS formulation (10) reads: find $\bar{u}\in\bar{V}$ such that

$$\begin{aligned}\int_\Omega(\kappa\nabla\bar{u}(x)-\beta\bar{u})\cdot\nabla\bar{v}(x)\,dx-\int_\Omega\int_\Omega\mathcal{L}\bar{u}(x)g'(x,y)\mathcal{L}^*\bar{v}(y)\,dxdy\\ =\int_\Omega f(x)\bar{v}(x)\,dx-\int_\Omega\int_\Omega f(x)g'(x,y)\mathcal{L}^*\bar{v}(y)\,dxdy,\qquad\forall\bar{v}\in\bar{V},\end{aligned} \tag{30}$$

Remark 1. *Note that here and in what follows the integrals have to be intended in the sense of distributions. We refer to [21] for details. Some explicit representations are given in [14].*

3.1 Linear elements and H_0^1-optimality in one dimension

Let $d=1$ and $\Omega=(0,L)$. Consider a grid of nodes $0=x_0<x_1<\ldots<x_{n_{el}-1}<x_{n_{el}}=L$ and the related subdivision of $(0,L)$ into n_{el} elements (x_{i-1},x_i), $i=1,\dots,n_{el}$ of size $h=L/n_{el}$. Let $\bar{V}\subset H_0^1$ be the space of piecewise-linear (with respect to the subdivision) functions, which is of dimension $N=n_{el}-1$.

In this context, the H_0^1-projector $\mathcal{P}=\mathcal{P}_{H_0^1}$ plays a special role. Indeed, it is easy to see that $(\mathcal{P}v)(x_i)=v(x_i)$, for all $i=1,\dots,N$. Actually, in this case it is well known in the literature (see [3, 8, 13, 14]) that the VMS approach provides a nodally exact approximation $\bar{u}$ of the exact solution u.

In order to have (27), we set $\mu_i=\delta(x-x_i)$. The abstract property (29) becomes, in this case,

$$g'(x,x_i)=g'(x_i,y)=0\qquad\forall i=1,\dots,N,\quad 0\le x,y\le L, \tag{31}$$

that is, g' vanishes if at least one of its two arguments is a node of the grid. Moreover, (28) gives

$$g'(x,y)=g(x,y)-\begin{bmatrix}g(x_1,y) & \dots & g(x_N,y)\end{bmatrix}\begin{bmatrix}g(x_1,x_1) & \dots & g(x_N,x_1)\\ \vdots & \ddots & \vdots\\ g(x_1,x_N) & \dots & g(x_N,x_N)\end{bmatrix}^{-1}\begin{bmatrix}g(x,x_1)\\ \vdots\\ g(x,x_N)\end{bmatrix}. \tag{32}$$

Recalling that $\mathcal{L}^*g(\cdot,y)=\delta(\cdot-y)$, from (32) we get

$$\begin{aligned}\mathcal{L}^*g'(\cdot,y)&=\delta(\cdot-y)-\begin{bmatrix}g(x_1,y) & \dots & g(x_N,y)\end{bmatrix}\begin{bmatrix}g(x_1,x_1) & \dots & g(x_N,x_1)\\ \vdots & \ddots & \vdots\\ g(x_1,x_N) & \dots & g(x_N,x_N)\end{bmatrix}^{-1}\begin{bmatrix}\delta(\cdot-x_1)\\ \vdots\\ \delta(\cdot-x_N)\end{bmatrix}\\ &=I+II.\end{aligned}$$

If $x_{i-1}<y<x_i$ then

$$\mathcal{L}^*g'(\cdot,y)=\delta(\cdot-y)\ \text{in}\ (x_{i-1},x_i), \tag{33}$$

while, when $y>x_i$ or $y<x_{i-1}$,

$$\mathcal{L}^*g'(\cdot,y)=0\ \text{in}\ (x_{i-1},x_i). \tag{34}$$

This, with (31), fully characterizes g': by (31) and (34), we see that $g'(x,y) = 0$ if x and y belong to two different elements; moreover, (31) and (33) say that g' is, on each $(x_{i-1}, x_i) \times (x_{i-1}, x_i)$, the so called *element* Green's function g^{el}, that is, the Green's function for the restriction of $\mathcal{L}$ to the element (x_{i-1}, x_i), with homogeneous Dirichlet boundary conditions at the endpoints x_{i-1} and x_i. Since $g'(x,y) \neq 0$ only when x and y belong to the same element, (26) can be localized within each element

$$u'(y) = \int_{x_{i-1}}^{x_i} g'(x,y) r(x)\, dx, \qquad \forall y \in (x_{i-1}, x_i). \tag{35}$$

See a plot of g' in Figure 1, where we consider the case of a uniform mesh of 16 elements (for $\kappa = 10^{-3}$, $\beta = 1$ and $L = 1$), and we compare with the plot of the Green's function g.

As said, the structure of g' for this case is well known in the literature [3, 8, 13, 14]. Indeed. recognizing that V' is the space of *bubbles*

$$V' = \bigoplus_{i=1,\dots,n_{el}} H_0^1(x_{i-1}, x_i), \tag{36}$$

the fine-scale variational equation (6) splits element by element, and admits the strong form

$$\mathcal{L}u' = f - \mathcal{L}\bar{u}, \text{ on } (x_{i-1}, x_i), \qquad \text{with } u'(x_{i-1}) = u'(x_i) = 0, \tag{37}$$

for each $i = 1, \dots, n_{el}$: u' is the solution of the advection-diffusion problem at the element level, with the coarse-scale residual acting as right-hand side. This is why $g' = g^{el}$, at the element level.

Moreover, assuming piecewise-constant coefficients κ, β and source term f, the fine-scale effect on the coarse-scale variational equation is

$$\begin{aligned} \int_0^L \int_0^L \mathcal{L}^* \bar{v}(y) g'(x,y) r(x)\, dxdy &= \sum_{i=1}^{n_{el}} \int_{x_{i-1}}^{x_i} \int_{x_{i-1}}^{x_i} \mathcal{L}^* \bar{v}(y) g'(x,y) r(x)\, dxdy \\ &= \sum_{i=1}^{n_{el}} \frac{\int_{x_{i-1}}^{x_i} \int_{x_{i-1}}^{x_i} g'(x,y)\, dxdy}{x_i - x_{i-1}} \int_{x_{i-1}}^{x_i} r(x) \mathcal{L}^* \bar{v}(x)\, dx, \end{aligned} \tag{38}$$

which is recognized as a classical stabilization term depending on the parameter [13, 14]

$$\tau_1 \equiv \tau_{1,(x_{i-1},x_i)} = \frac{\int_{x_{i-1}}^{x_i} \int_{x_{i-1}}^{x_i} g'(x,y)\, dxdy}{x_i - x_{i-1}}. \tag{39}$$

We recall (from [13, 14]) that the expression of $g'(x,y) = g^{el}(x,y)$ on $(0,h) \times (0,h)$ is:

$$g^{el}(x,y) = \begin{cases} \dfrac{\left(1 - e^{-\frac{\beta h}{\kappa}\left(1 - \frac{y}{h}\right)}\right)\left(1 - e^{-\frac{\beta x}{\kappa}}\right)}{\beta\left(1 - e^{-\frac{\beta h}{\kappa}}\right)} & \text{if } x \leq y, \\ \dfrac{\left(e^{\frac{\beta y}{\kappa}} - 1\right)\left(e^{-\frac{\beta x}{\kappa}} - e^{-\frac{\beta h}{\kappa}}\right)}{\beta\left(1 - e^{-\frac{\beta h}{\kappa}}\right)} & \text{if } x \geq y. \end{cases} \tag{40}$$

Introducing the mesh Peclét number

$$\alpha = \frac{h\beta}{2\kappa},$$

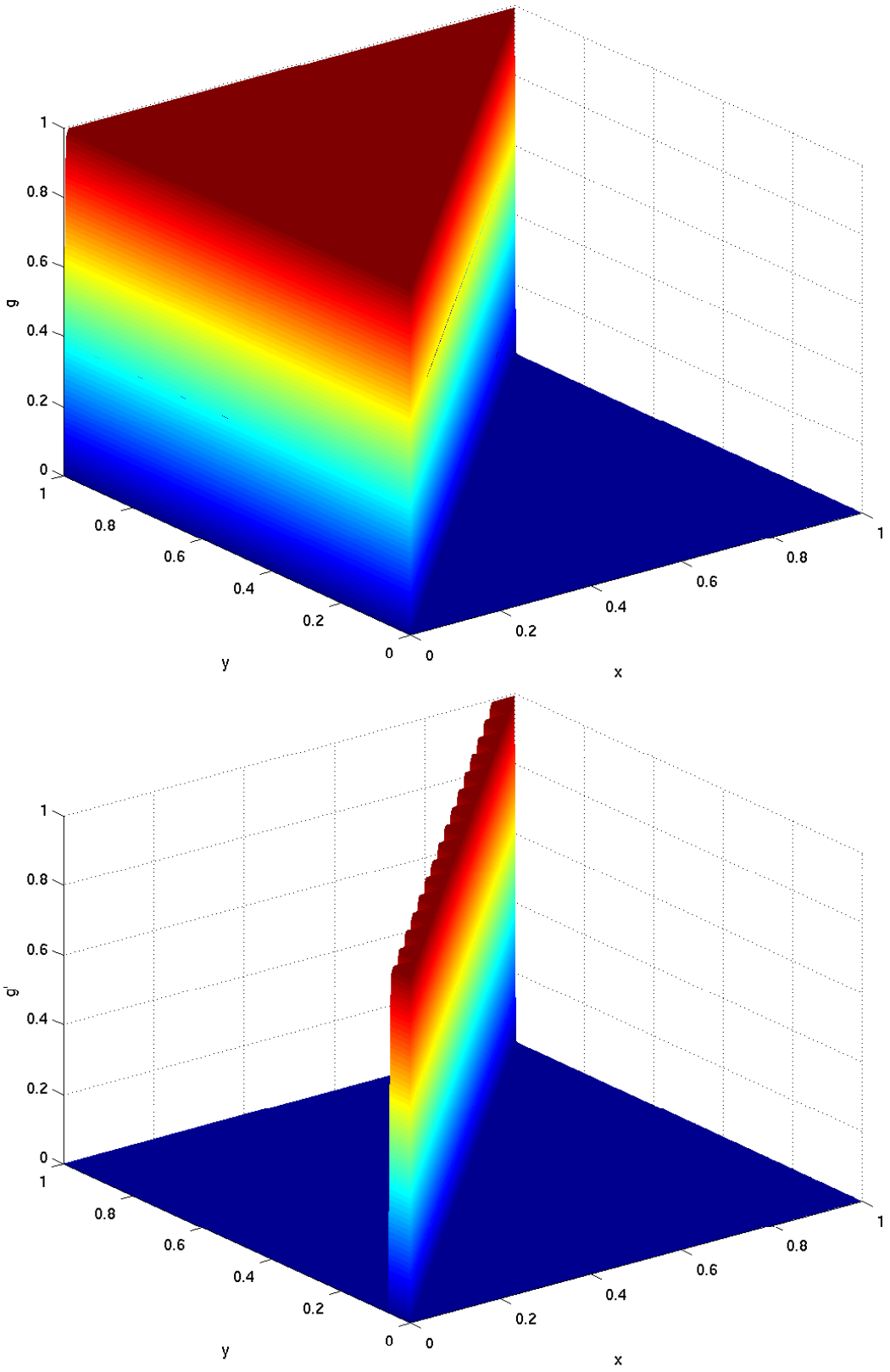

Figure 1: Comparison between the Green's function g (above) and the fine-scale Green's function g' (below) for the one-dimensional problem and linear elements, with $\mathcal{P} = \mathcal{P}_{H_0^1}$, $\kappa = 10^{-3}$, $\beta = 1$, $L = 1$ and a uniform grid of $n_{el} = 16$ elements. Note that the support of g' is local in that there is no coupling between elements. This is an advantage of $\mathcal{P} = \mathcal{P}_{H_0^1}$.

one obtains the canonical result

$$\begin{aligned}\tau_1 &= \frac{h}{2\beta}\frac{(e^{2\alpha}-\alpha^{-1}e^{2\alpha}+1+\alpha^{-1})}{(e^{2\alpha}-1)} \\ &= \frac{h}{2\beta}\left(\coth(\alpha)+\frac{1}{\alpha}\right).\end{aligned} \tag{41}$$

We show plots of g' on $(0,h)\times(0,h)$ in the diffusive and in the advective regime in Figure 2. A plot of τ_1 is presented in Figure 5.

3.2 Higher-order elements and H_0^1-optimality in one dimension

We consider now higher-order piecewise-polynomial coarse scales on the grid $0 = x_0 < x_1 < \ldots < x_{n_{el}-1} < x_{n_{el}} = L$, that is, we set

$$\bar{V} = \left\{\bar{v} \in H_0^1(0,L) \text{ such that } \bar{v}_{|(x_{i-1},x_i)} \in \mathbb{P}_k,\ 1 \le i \le n_{el}\right\},$$

where $\mathbb{P}_k$ is the space of polynomials of degree at most k. We still deal with $\mathcal{P} = \mathcal{P}_{H_0^1}$. The case of higher-order elements ($k \ge 2$) has not been studied in the literature of VMS methods, as far as we know. There are indeed additional difficulties with respect to the case of linear elements: V' is still a space of bubbles, but, unlike the case $k = 1$, $\bar{V}$ also contains some (polynomial) bubbles, which are therefore missing in V'. This means that V' is a strict subset of bubbles

$$V' \underset{\neq}{\subset} \bigoplus_{i=1,\ldots,n_{el}} H_0^1(x_{i-1},x_i), \tag{42}$$

or, equivalently, V' is a space of bubbles with additional constraints. As a result, the fine-scale variational equation (6) can still be split element by element into

$$\int_{x_{i-1}}^{x_i} \mathcal{L}u'(x)v'(x)\,dx = \int_{x_{i-1}}^{x_i} (f(x)-\mathcal{L}\bar{u}(x))v'(x)\,dx, \qquad \forall v' \in V', \quad i = 1,\ldots,n_{el}, \tag{43}$$

however, (43) is no longer equivalent to the strong form (37).

We can use the theory of Section 2 for dealing with (43). Taking advantage of (42), we restrict from the beginning to a single element (x_{i-1},x_i) and to the bubbles supported on it. Then, we take as the fine-scale space $V_i' = V'_{|(x_{i-1},x_i)}$. The space of the bubbles which are polynomials of degree at most k plays the role of a coarse space on (x_{i-1},x_i): we set $\bar{V}_i = \bar{V}_{|(x_{i-1},x_i)} \cap H_0^1(x_{i-1},x_i)$. The space of unconstrained bubbles is $V_i = H_0^1(x_{i-1},x_i) = \bar{V}_i \oplus V_i'$. Precisely $w \in V_i$ belongs to V_i' if and only if (integrating by parts)

$$0 = \int_{x_{i-1}}^{x_i} \frac{d}{dx}w(x)\frac{d}{dx}\bar{v}(x)\,dx = -\int_{x_{i-1}}^{x_i} w(x)\frac{d^2}{dx^2}\bar{v}(x)\,dx, \qquad \forall \bar{v} \in \bar{V}_i. \tag{44}$$

The second-order derivatives of $\bar{V}_i$ functions are the polynomials of degree at most $k-2$. We need, as $\{\mu_j\}_{j=1,\ldots,N}$ (where $N = k-1$, now) a basis of $\mathbb{P}_{k-2}$. For example, we can set

$$\mu_j(x) = (x-x_{i-1})^{j-1}, \qquad 1 \le j \le N.$$

The constraint is expressed, as in (19), by N scalar equations: $v \in V_i$ belongs to V_i' if and only if

$$\int_{x_{i-1}}^{x_i} \mu_j(x)v(x)\,dx, \qquad 1 \le j \le N. \tag{45}$$

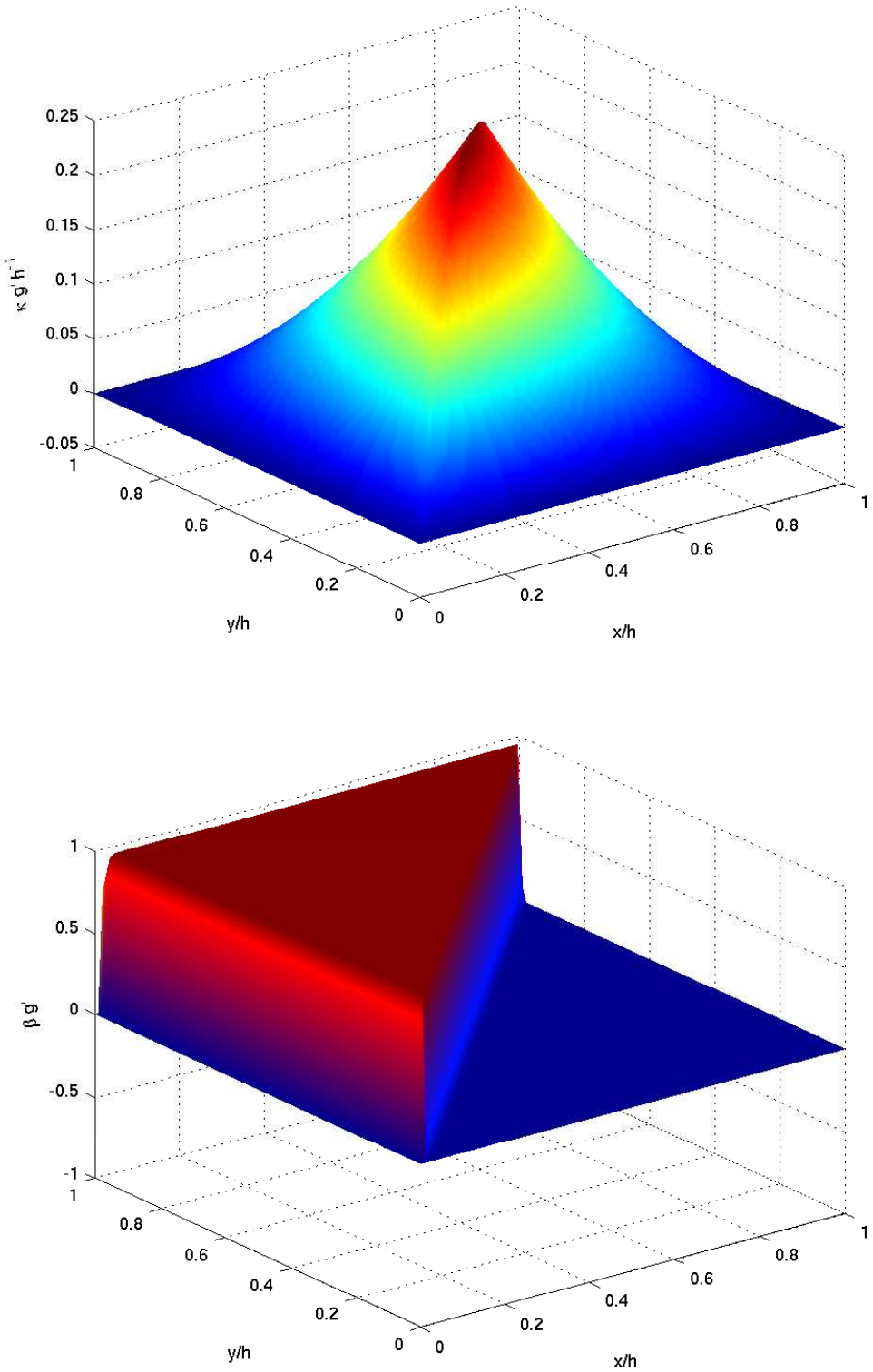

Figure 2: Fine-scale Green's functions g' at the element level $(0,h)\times(0,h)$, for the one-dimensional problem and linear elements. In the diffusive regime $\alpha = 10^{-2}$ (above), and in the advective regime $\alpha = 10^{2}$ (below). $\mathcal{P} = \mathcal{P}_{H_0^1}$.

The Green's function of the unconstrained bubble problem is the element Green's function g^{el} given in (40). Then, we can now use the formula (22) and derive an expression for g' in terms of g^{el}: on $(0,h)\times(0,h)$ we have

$$\begin{aligned} g'(x,y) = g^{el}(x,y) &- \left[\int_0^h g^{el}(\tilde{x},y)d\tilde{x} \quad \dots \quad \int_0^h \tilde{x}^{k-2} g^{el}(\tilde{x},y)d\tilde{x}\right] \\ &\times \begin{bmatrix} \int_0^h\int_0^h g^{el}(\tilde{x},\tilde{y})d\tilde{x}d\tilde{y} & \dots & \int_0^h\int_0^h \tilde{x}^{k-2} g^{el}(\tilde{x},\tilde{y})d\tilde{x}d\tilde{y} \\ \vdots & \ddots & \vdots \\ \int_0^h\int_0^h \tilde{y}^{k-2} g^{el}(\tilde{x},\tilde{y})d\tilde{x}d\tilde{y} & \dots & \int_0^h\int_0^h \tilde{x}^{k-2}\tilde{y}^{k-2} g^{el}(\tilde{x},\tilde{y})d\tilde{x}d\tilde{y} \end{bmatrix}^{-1} \\ &\times \begin{bmatrix} \int_0^h g^{el}(x,\tilde{y})d\tilde{y} \\ \vdots \\ \int_0^h \tilde{y}^{k-2} g^{el}(x,\tilde{y})d\tilde{y} \end{bmatrix}. \end{aligned} \tag{46}$$

We recall that $g'(x,y)=0$ if x and y belongs to different elements, while g' on each $(x_{i-1},x_i)\times(x_{i-1},x_i)$ can be obtained from (46) straightforwardly.

We discuss now more in detail the case of quadratic ($k=2$) and cubic ($k=3$) coarse-scale elements. If $k=2$ then (46) yields

$$g'(x,y) = g^{el}(x,y) - \frac{\int_0^h g^{el}(\tilde{x},y)d\tilde{x}\int_0^h g^{el}(x,\tilde{y})d\tilde{y}}{\int_0^h\int_0^h g^{el}(\tilde{x},\tilde{y})d\tilde{x}d\tilde{y}} = I + II. \tag{47}$$

Then g' is the sum of the element Green's function (term I) and a correction II. Assuming positive and piecewise-constant coefficients κ and β,

$$\int_0^h g^{el}(\tilde{x},y)d\tilde{x} = \frac{\left(ye^{\frac{\beta h}{\kappa}} - he^{\frac{\beta y}{\kappa}} + h - y\right)}{\beta\left(e^{\frac{\beta h}{\kappa}} - 1\right)},$$

$$\int_0^h g^{el}(x,\tilde{y})d\tilde{y} = -\frac{\left(-x - he^{\frac{\beta h}{\kappa}} + e^{-\frac{\beta(-h+x)}{\kappa}}h + e^{\frac{\beta h}{\kappa}}x\right)}{\beta\left(e^{\frac{\beta h}{\kappa}} - 1\right)},$$

$$\int_0^h\int_0^h g^{el}(\tilde{x},\tilde{y})d\tilde{x}d\tilde{y} = \frac{h\left(he^{\frac{\beta h}{\kappa}}\beta - 2\,e^{\frac{\beta h}{\kappa}}\kappa + \beta h + 2\,\kappa\right)}{2\beta^2\left(e^{\frac{\beta h}{\kappa}} - 1\right)},$$

and then II becomes

$$II = \frac{2\left(ye^{\frac{\beta h}{\kappa}} - he^{\frac{\beta y}{\kappa}} + h - y\right)\left(-x - he^{\frac{\beta h}{\kappa}} + e^{-\frac{\beta(-h+x)}{\kappa}}h + e^{\frac{\beta h}{\kappa}}x\right)}{h\left(e^{\frac{\beta h}{\kappa}} - 1\right)\left(he^{\frac{\beta h}{\kappa}}\beta - 2\,e^{\frac{\beta h}{\kappa}}\kappa + \beta h + 2\,\kappa\right)}.$$

Plots of g' on $(0,h)\times(0,h)$ for quadratic elements are shown in Figure 3.

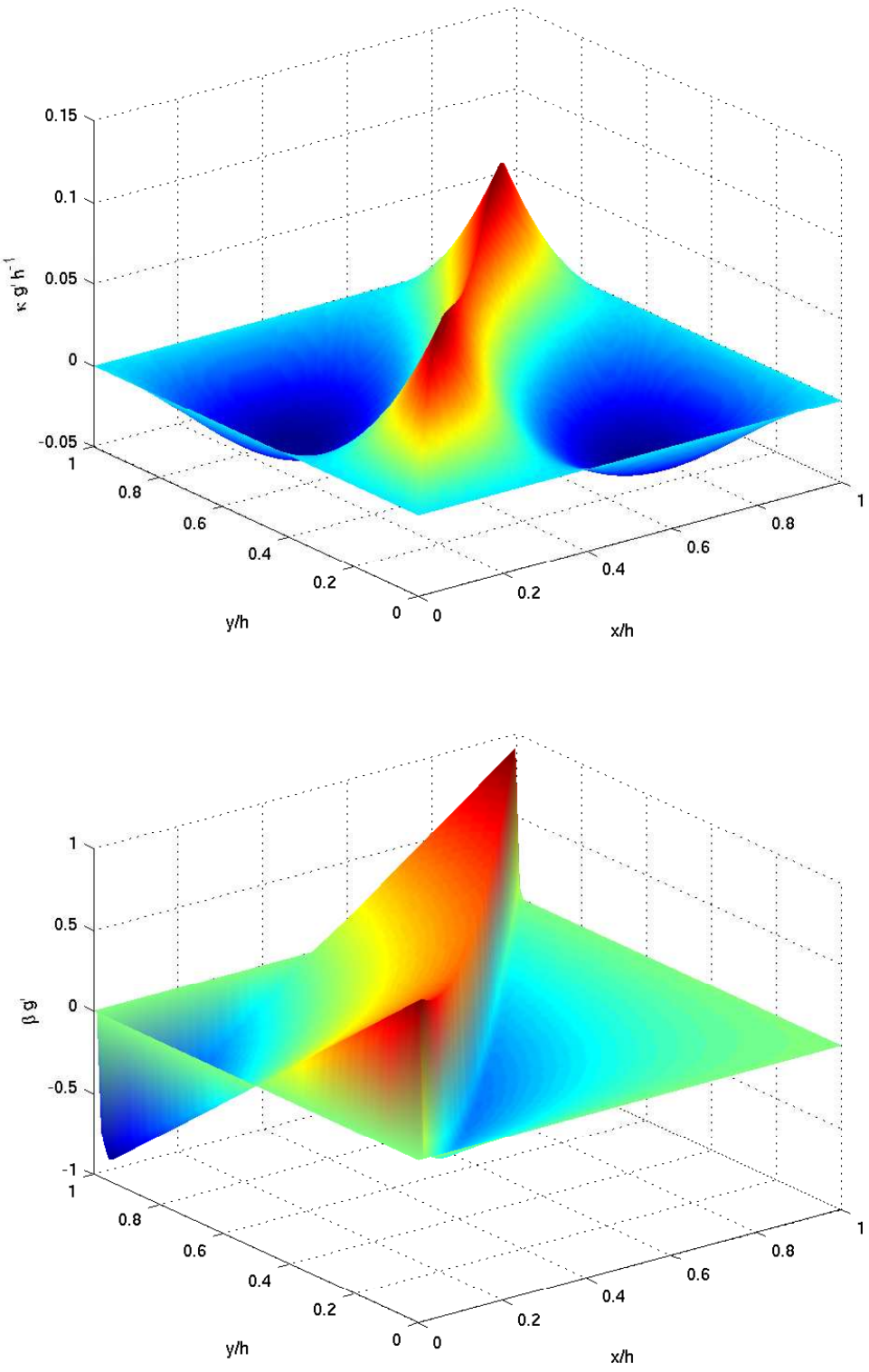

Figure 3: Fine-scale Green's functions g' at the element level $(0,h)\times(0,h)$, for the one-dimensional problem and quadratic elements. In the diffusive regime $\alpha = 10^{-2}$ (above), and in the advective regime $\alpha = 10^{2}$ (below). $\mathcal{P} = \mathcal{P}_{H_0^1}$.

For $k=3$, (46) gives

$$
\begin{aligned}
g'(x,y) = g^{el}(x,y) &- \begin{bmatrix} \int_0^h g^{el}(\tilde{x},y)d\tilde{x} & \int_0^h \tilde{x} g^{el}(\tilde{x},y)d\tilde{x} \end{bmatrix} \\
&\times \begin{bmatrix} \int_0^h \int_0^h g^{el}(\tilde{x},\tilde{y})d\tilde{x}d\tilde{y} & \int_0^h \int_0^h \tilde{x} g^{el}(\tilde{x},\tilde{y})d\tilde{x}d\tilde{y} \\ \int_0^h \int_0^h \tilde{y} g^{el}(\tilde{x},\tilde{y})d\tilde{x}d\tilde{y} & \int_0^h \int_0^h \tilde{x}\tilde{y} g^{el}(\tilde{x},\tilde{y})d\tilde{x}d\tilde{y} \end{bmatrix}^{-1} \\
&\times \begin{bmatrix} \int_0^h g^{el}(x,\tilde{y})d\tilde{y} \\ \int_0^h \tilde{y} g^{el}(x,\tilde{y})d\tilde{y} \end{bmatrix} \\
&= I + III.
\end{aligned}
\tag{48}
$$

Now the correction term III is

$$
\begin{aligned}
III = 6\,h^{-3} \Big[& 2\,h^4\kappa e^{\frac{\beta h}{\kappa}} + 2\,e^{\frac{\beta h}{\kappa}}\beta y^2 h^2 x - 12\,e^{\frac{\beta h}{\kappa}} y h\kappa x^2 - 2\,y\beta h^2 e^{\frac{\beta h}{\kappa}} x^2 \\
& + \beta h^3 e^{\frac{\beta h}{\kappa}} x^2 - \beta y^2 h^3 e^{\frac{\beta h}{\kappa}} + \beta y^2 h^3 e^{-\frac{\beta(-h+x)}{\kappa}} - \beta h^4 e^{\frac{\beta h}{\kappa}} x + h^3 e^{\frac{\beta y}{\kappa}} \beta x^2 \\
& - 2\,h^3 e^{\frac{\beta y}{\kappa}} x\kappa - 12\,y^2 e^{\frac{\beta h}{\kappa}} h\kappa x + 16\,e^{\frac{\beta h}{\kappa}} y h^2 \kappa x - 2\,h^3 e^{\frac{\beta h}{\kappa}} x\kappa \\
& - 2\,y h^3 \kappa e^{\frac{\beta h}{\kappa}} + 2\,y h^3 \kappa e^{-\frac{\beta(-h+x)}{\kappa}} + y\beta h^4 e^{\frac{\beta h}{\kappa}} - y\beta h^4 e^{-\frac{\beta(-h+x)}{\kappa}} \\
& + 12\,y^2 \kappa e^{\frac{\beta h}{\kappa}} x^2 - h^4 e^{\frac{\beta y}{\kappa}} \beta x - 2\,e^{-\frac{\beta(-2\,h+x)}{\kappa}} y h^3 \kappa - \beta y^2 e^{-\frac{\beta(-2\,h+x)}{\kappa}} h^3 \\
& + h^4 e^{\frac{\beta(h+y)}{\kappa}} \beta x + 2\,h^3 e^{\frac{\beta(h+y)}{\kappa}} x\kappa + 3\,\beta y^2 e^{2\,\frac{\beta h}{\kappa}} h x^2 - 2\,e^{2\,\frac{\beta h}{\kappa}} y\beta h^2 x^2 \\
& + 6\,y^2 e^{2\,\frac{\beta h}{\kappa}} h\kappa x + \beta y^2 e^{2\,\frac{\beta h}{\kappa}} h^3 + 3\,e^{2\,\frac{\beta h}{\kappa}} y\beta h^3 x + 6\,e^{2\,\frac{\beta h}{\kappa}} y\kappa h x^2 \\
& - 8\,e^{2\,\frac{\beta h}{\kappa}} y h^2 \kappa x - h^3 e^{\frac{\beta(h+y)}{\kappa}} \beta x^2 - e^{2\,\frac{\beta h}{\kappa}} y\beta h^4 + 2\,e^{2\,\frac{\beta h}{\kappa}} y h^3 \kappa \\
& - 2\,h^4 e^{\frac{\beta(h+y)}{\kappa}} \kappa + 2\,h^4 e^{\frac{\beta(y+h-x)}{\kappa}} \kappa + e^{-\frac{\beta(-2\,h+x)}{\kappa}} y\beta h^4 - 6\,y^2 e^{2\,\frac{\beta h}{\kappa}} \kappa x^2 \\
& - 4\,\beta y^2 e^{2\,\frac{\beta h}{\kappa}} h^2 x - 2\,h^4 \kappa e^{-\frac{\beta(-h+x)}{\kappa}} - 6\,y^2 \kappa x^2 + \beta h^4 x + 6\,y^2 h x\kappa \\
& - 3\,\beta y^2 h x^2 - \beta h^3 x^2 + 6\,y h\kappa x^2 - 8\,y h^2 x\kappa + 4\,y\beta h^2 x^2 + 2\,h^3 x\kappa \\
& + 2\,\beta y^2 h^2 x - 3\,y\beta h^3 x \Big] \cdot \left[e^{\frac{\beta h}{\kappa}} - 1 \right]^{-1} \\
\cdot \Big[& \beta^2 h^2 e^{\frac{\beta h}{\kappa}} + 12\,e^{\frac{\beta h}{\kappa}} \kappa^2 - 6\,e^{\frac{\beta h}{\kappa}} h\kappa\beta - \beta^2 h^2 - 12\,\kappa^2 - 6\,\beta h\kappa \Big]^{-1}.
\end{aligned}
$$

The expression for III was obtained by a symbolic MATLAB evaluation and is elaborate. More significant are the plots of g' provided, for cubic elements ($k=3$), in Figure 4.

Observe that, from (20)–(21), g' is orthogonal to $\mathbb{P}_{k-2}$ with respect to each variable x and y, on each $(x_{i-1},x_i)\times(x_{i-1},x_i)$. Still assuming that the coefficients κ and β are piecewise-constant and the source term f is a piecewise-polynomial of degree at most $k-1$, then on (x_{i-1},x_i) we have

$$
r(x) = \frac{d^{k-1}r}{dx^{k-1}} \frac{x^{k-1}}{(k-1)!} + \text{ “polynomial of degree } \le k-2\text{”},
$$

and

$$
\mathcal{L}^*\bar{v}(y) = \frac{d^{k-1}\mathcal{L}^*\bar{v}}{dx^{k-1}} \frac{y^{k-1}}{(k-1)!} + \text{ “polynomial of degree } \le k-2\text{”}.
$$

Therefore, exploiting both the locality and the orthogonality of g' with respect to polynomials of

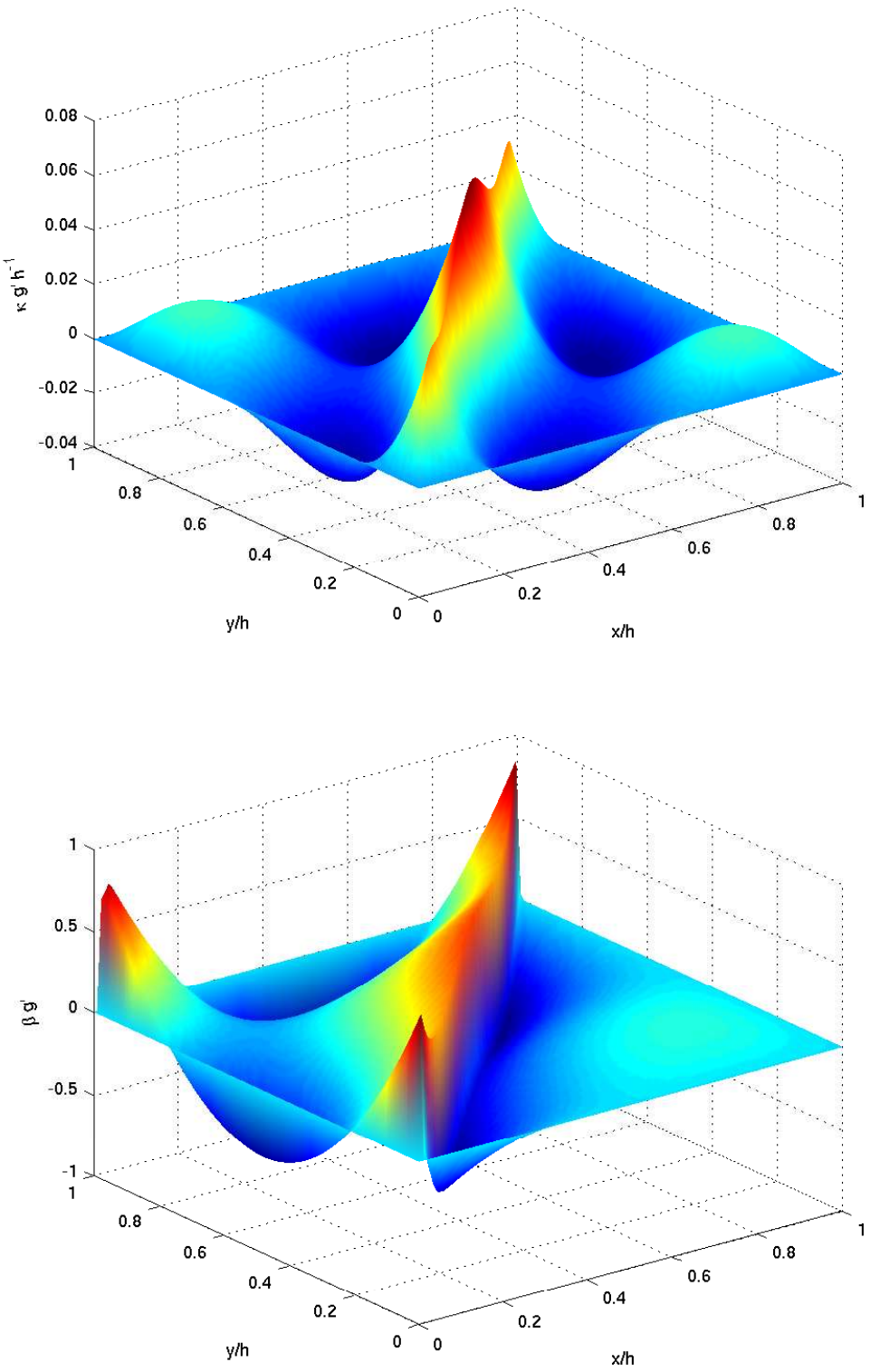

Figure 4: Fine-scale Green's functions g' at the element level $(0,h)\times(0,h)$, for the one-dimensional problem and cubic elements. In the diffusive regime $\alpha = 10^{-2}$ (above), and in the advective regime $\alpha = 10^{2}$ (below). $\mathcal{P} = \mathcal{P}_{H_0^1}$.

degree $k-2$, the fine-scale effect on the coarse-scale equation can be written as

$$\begin{aligned}
&\int_0^L \int_0^L \mathcal{L}^*\bar{v}(y)g'(x,y)r(x)\,dxdy \\
&\quad= \sum_{i=1}^{n_{el}} \int_{x_{i-1}}^{x_i} \int_{x_{i-1}}^{x_i} \mathcal{L}^*\bar{v}(y)g'(x,y)r(x)\,dxdy \\
&\quad= \frac{1}{((k-1)!)^2} \sum_{i=1}^{n_{el}} \int_{x_{i-1}}^{x_i} \int_{x_{i-1}}^{x_i} y^{k-1} \frac{d^{k-1}\mathcal{L}^*\bar{v}}{dx^{k-1}} g'(x,y) x^{k-1} \frac{d^{k-1}r}{dx^{k-1}}\,dxdy \\
&\quad= \sum_{i=1}^{n_{el}} \frac{\int_{x_{i-1}}^{x_i}\int_{x_{i-1}}^{x_i} y^{k-1}g'(x,y)x^{k-1}dxdy}{((k-1)!)^2\,(x_i - x_{i-1})} \int_{x_{i-1}}^{x_i} \frac{d^{k-1}r}{dx^{k-1}} \frac{d^{k-1}\mathcal{L}^*\bar{v}}{dx^{k-1}}\,dx \\
&\quad= \sum_{i=1}^{n_{el}} \tau_{k,(x_{i-1},x_i)} \int_{x_{i-1}}^{x_i} \frac{d^{k-1}r}{dx^{k-1}} \frac{d^{k-1}\mathcal{L}^*\bar{v}}{dx^{k-1}}\,dx.
\end{aligned} \tag{49}$$

The stabilization term only acts locally and only depends on the derivative of degree $k-1$ of the residual; its effect is modulated by the parameter

$$\tau_k \equiv \tau_{k,(x_{i-1},x_i)} = \frac{\int_{x_{i-1}}^{x_i}\int_{x_{i-1}}^{x_i} y^{k-1}g'(x,y)x^{k-1}dxdy}{((k-1)!)^2\,(x_i - x_{i-1})}.$$

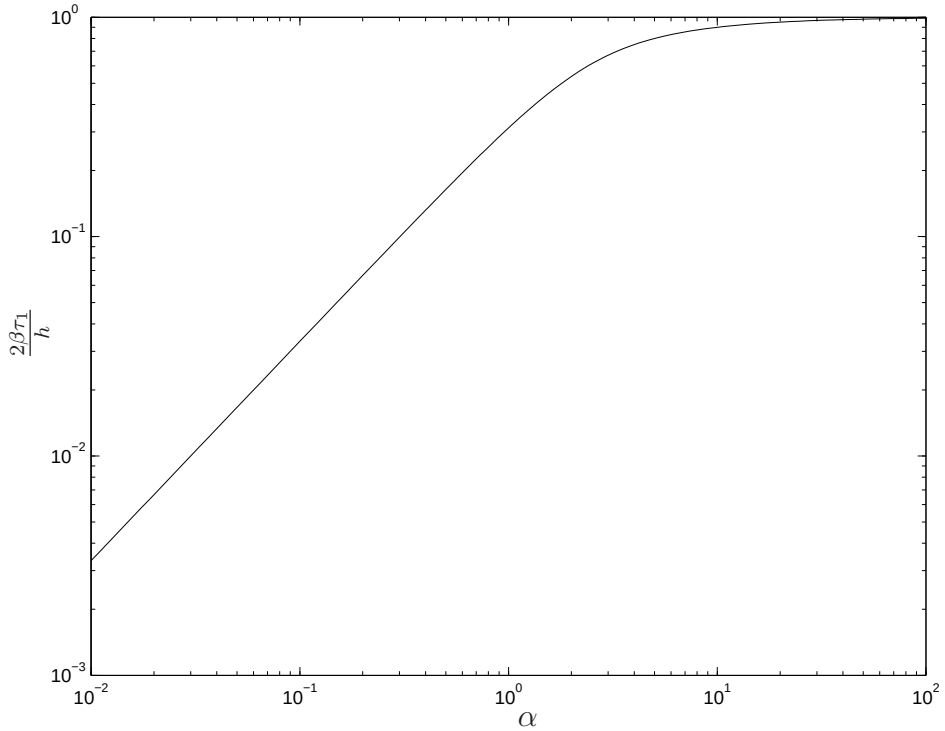

Figure 5: Stabilization parameter τ_1 versus α.

In the case of quadratic elements ($k=2$), from the previous formulas one can derive

$$\tau_2 = \frac{h^3}{72\,\beta} \frac{-3e^{2\alpha}\alpha^{-1} + e^{2\alpha} + 3e^{2\alpha}\alpha^{-2} - 3\alpha^{-2} - 1 - \alpha^{-1}}{e^{2\alpha} - e^{2\alpha}\alpha^{-1} + 1 + \alpha^{-1}}, \tag{50}$$

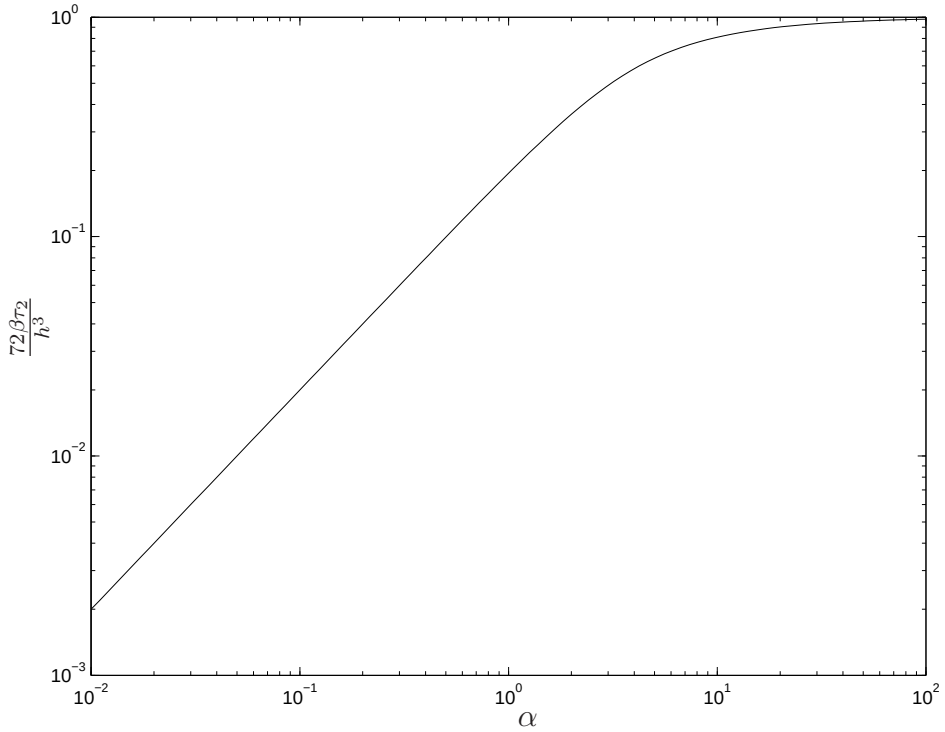

Figure 6: Stabilization parameter τ_2 versus α.

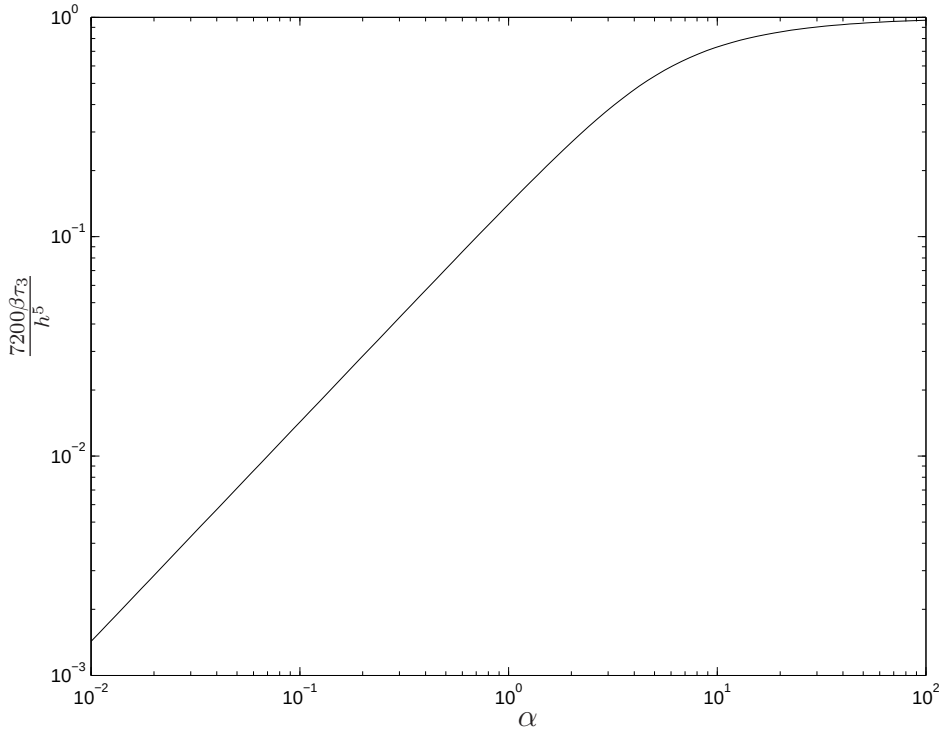

Figure 7: Stabilization parameter τ_3 versus α.

while, for cubic elements ($k = 3$),

$$\tau_3 = \frac{h^5}{7200\,\beta}\,\frac{15e^{2\alpha}\alpha^{-2} - 6e^{2\alpha}\alpha^{-1} - 15e^{2\alpha}\alpha^{-3} + e^{2\alpha} + 15\alpha^{-3} + 6\alpha^{-1} + 15 + 1}{e^{2\alpha} - 3e^{2\alpha}\alpha^{-1} + 3e^{2\alpha}\alpha^{-2} - 1 - 3\alpha^{-2} - 3\alpha^{-1}} \tag{51}$$

Plots of τ_2 and τ_3 are presented in Figure 6–7.

Remark 2. *From Figure 5–7 we see that the τ_k are positive and of order h^{2k-1}/β and $\alpha h^{2k-1}/\beta = h^{2k}/\kappa$ in the advective and in the diffusive regimes, respectively.*

Remark 3. *For linear elements, in one dimension, the H^1_0-optimal $\bar{u}$ is the nodal interpolant of u, which is a monotonicity preserving approximant. For higher-order elements, the H^1_0-optimal $\bar{u}$ is still nodally exact at the endpoints of each element, but we lose monotonicity inside the elements.*

Remark 4. *The format of (49) is reminiscent of the gradient least-squares stabilized method proposed by Franca and Dutra do Carmo [10].*

3.3 L^2-optimality in one dimension and the localization of g'

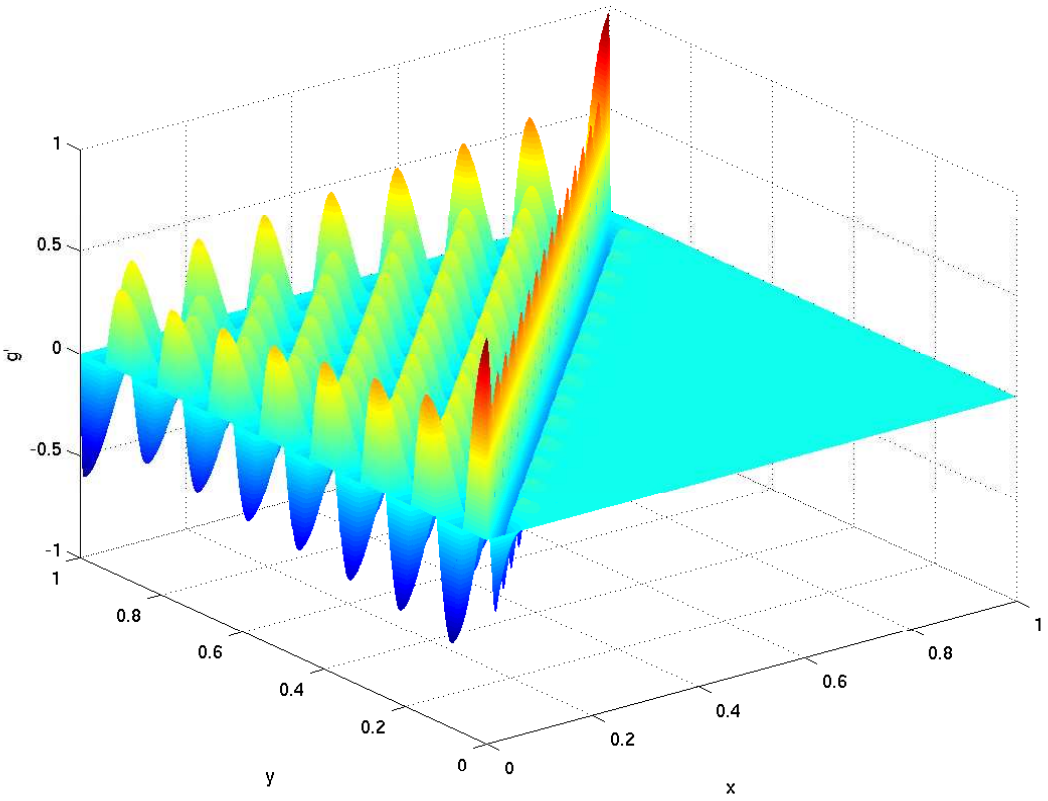

Figure 8: Fine-scale Green's function g' for the one-dimensional problem and linear elements, with $\mathcal{P} = \mathcal{P}_{L^2}$, $\kappa = 10^{-3}$, $\beta = 1$, $L = 1$ and a uniform grid of $n_{el} = 16$ elements. Note that in the case of $\mathcal{P} = \mathcal{P}_{L^2}$, g' is global and unattenuated when advection dominates.

We have shown that, for the one-dimensional problem and for the H^1_0-projector based VMS formulation (i.e., with $\mathcal{P} = \mathcal{P}_{H^1_0}$), the fine-scale Green's function is supported on the union of the

$(x_{i-1}, x_i) \times (x_{i-1}, x_i)$, for $1 \leq i \leq n_{el}$. In this case, the g' is *fully localized* within each element, in that there is no coupling between elements. This allows a convenient evaluation of the fine-scale effect in the VMS formulation (see (38) and (49)). This feature, though, is not guaranteed for any projector $\mathcal{P}$. Take, for example, the L^2-projector $\mathcal{P} = \mathcal{P}_{L^2}$, with piecewise-linear elements. We can still compute g' from (28), where now, in order to have (27), $\{\mu_i\}_{i=1,\ldots,N}$ is a basis for $\bar{V}$ itself. For $\kappa = 10^{-3}$, $\beta = 1$, $L = 1$ and $n_{el} = 16$ elements, a plot of g' is presented in Figure 8: we see that the support of g' includes the entire upwind region $x \leq y$.

Remark 5. *In practical applications, g' needs to be approximated, leading to classical stabilized methods. It is obviously more convenient and easy to approximate a highly-localized g' than one that is global. This strongly suggests that the selection of the projector is crucial in the development of a multiscale method.*

3.4 Linear elements in two dimensions

Turning to problems in two dimensions (as well as in multiple dimensions), we face two important differences.

First, it is technical and more difficult to obtain the analytical expression of the Green's function g, and therefore of the fine-scale Green's function g' through (28). To overcome this difficulty, in this section we propose to numerically compute g and g' on a fine mesh of $512 \times 512 \times 2$ elements, which is able to resolve the fine scales of the problem under consideration. We take here $\Omega = (0,1)^2$, the diffusivity is $\kappa = 10^{-3}$, and the unit advection velocity is $\beta = [1/2 \quad 1]/\sqrt{1.25}$. Since both g and g' are defined on $(0,1)^2 \times (0,1)^2$, for the purposes of a graphical representation we fix $y = y^* = [39/64 \quad 51/64] \approx [0.6 \quad 0.8]$ (see Figure 9) and we plot the Green's function g and fine-scale Green's function g' versus the argument x. The plot of $x \mapsto g(x, y^*)$ is presented in Figure 10. As is known, $x \mapsto g(x, y^*)$ is singular when $x = y^*$, and indeed the graph in Figure 10 has been truncated at $g = 50$. Roughly speaking, g is supported around the upwind characteristic passing through y^*.

The second major difference, compared to the one-dimensional case, is that if the coarse scales are piecewise-polynomial, then the fine scales are not localized within each element (i.e., they are not bubble functions), and this happens for any choice of projector $\mathcal{P}$, including the H_0^1-projector. Indeed, since the coarse scales are polynomials on the edges of the elements of the triangulation, while the exact solution is arbitrary, the fine scales do not vanish there. Our aims here are the calculation of g' and the assessment of its attenuation compared with g and its locality for different choices of $\mathcal{P}$. We test both $\mathcal{P} = \mathcal{P}_{H_0^1}$ and $\mathcal{P} = \mathcal{P}_{L^2}$, which gave, in the one-dimensional case, a fully-localized and a globally-supported g', respectively. We take the space $\bar{V}$ formed by linear elements on the uniform triangulation shown in Figure 9. The plots of $x \mapsto g'(x, y^*)$ for $\mathcal{P} = \mathcal{P}_{H_0^1}$ and $\mathcal{P} = \mathcal{P}_{L^2}$ are presented in Figures 11 and 12, respectively. The singularity at $x = y^*$ is still truncated at $g' = 50$. Observe that in the case $\mathcal{P} = \mathcal{P}_{H_0^1}$, the fine-scale Green's function is more localized around y^*, compared with the case $\mathcal{P} = \mathcal{P}_{L^2}$, for which oscillations are spread over the entire domain. In addition, the g' for the case $\mathcal{P} = \mathcal{P}_{H_0^1}$ seems to be negligible outside a layer of a few elements around y^*. This is better seen in the two-dimensional contour plots of $x \mapsto g'(x, y^*)$ in Figure 14 and 15, where the coarse mesh is overlaid. The two-dimensional plot of $x \mapsto g(x, y^*)$ is given for reference in Figure 13.

Changing the position of y^* inside Ω, and taking y^* on an edge or a vertex of the coarse triangulation, produces similar results (not shown).

Remark 6. *The upwind tail of g is global in the advection-dominated case, whereas it is highly*

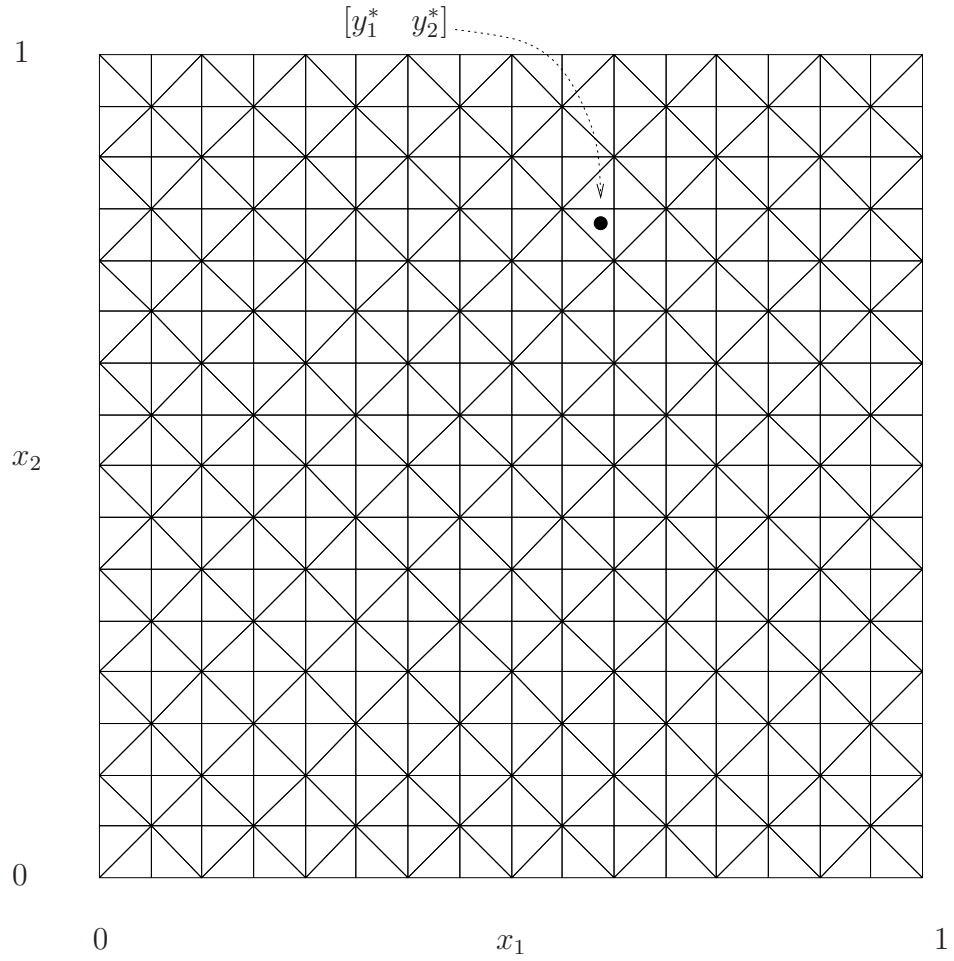

Figure 9: Mesh of the coarse-scale space $\bar{V}$ used for the calculation of the Green's functions in the two-dimensional case, and location of $y^* = [y_1^* \quad y_2^*]$.

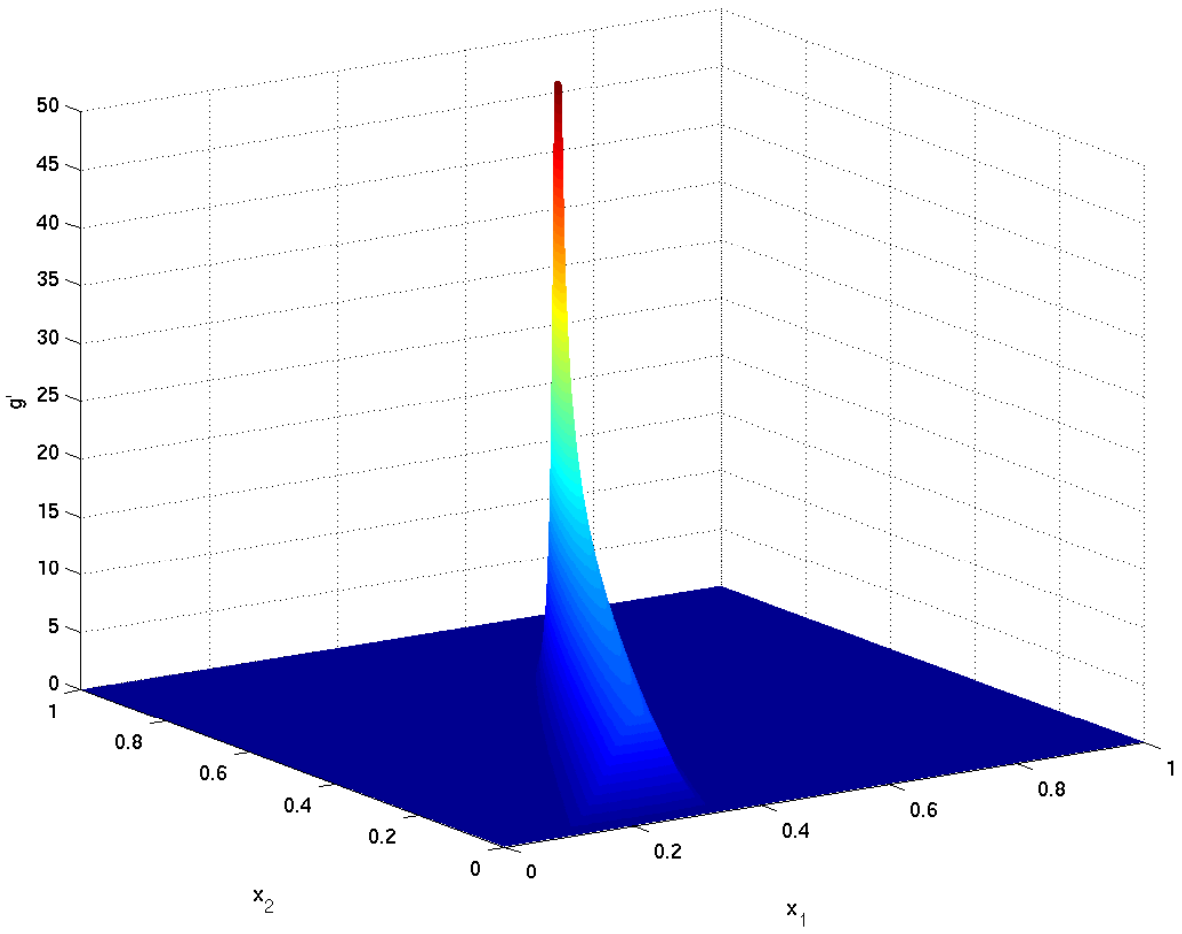

Figure 10: Plot of $x \mapsto g(x, y^*)$, for $g \leq 50$.

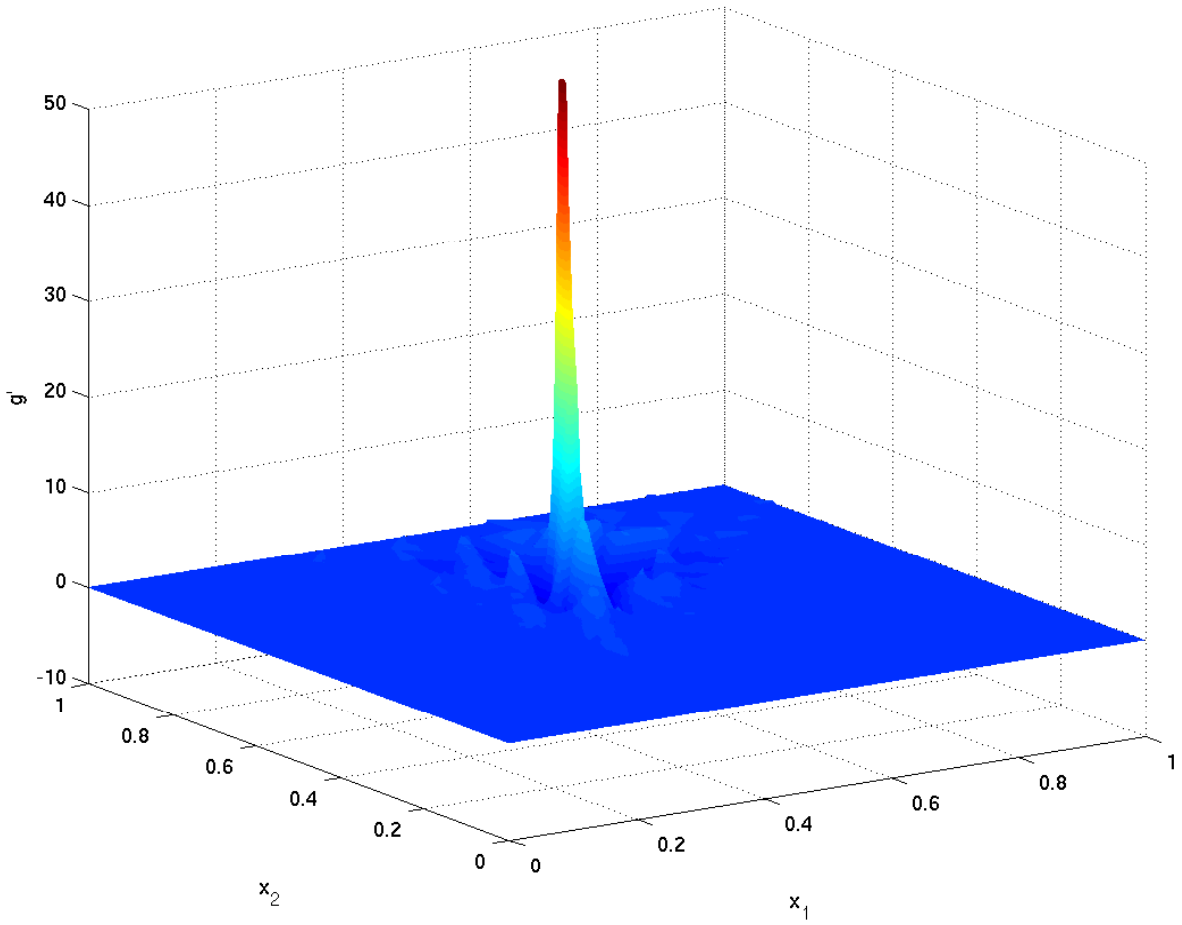

Figure 11: Plot of $x \mapsto g'(x, y^*)$ for $\mathcal{P} = \mathcal{P}_{H_0^1}$, and $g' \leq 50$.

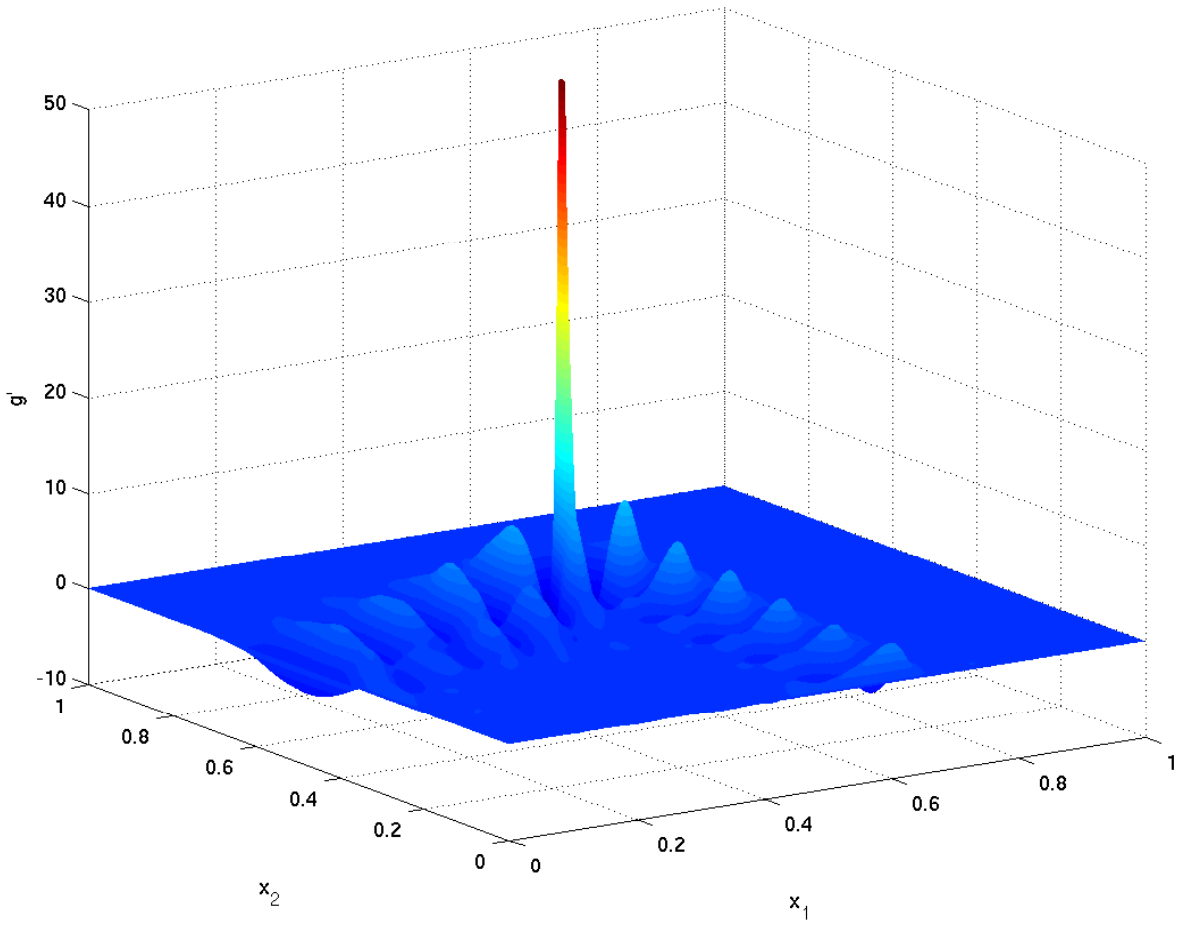

Figure 12: Plot of $x \mapsto g'(x, y^*)$ for $\mathcal{P} = \mathcal{P}_{L^2}$, and $g' \leq 50$.

attenuated for g' when $\mathcal{P} = \mathcal{P}_{H_0^1}$ (cf. Fig. 10 with 11, and Fig. 13 with 14). This has important implications for multiscale analysis of dominantly-hyperbolic phenomena. In addition, the g' for $\mathcal{P} = \mathcal{P}_{H_0^1}$ is much more localized than that for $\mathcal{P} = \mathcal{P}_{L^2}$. These results are consistent with the one-dimensional case and suggest that local approximations of g' for $\mathcal{P} = \mathcal{P}_{H_0^1}$ may achieve near H_0^1-optimality in multi-dimensional, advection-dominated cases.

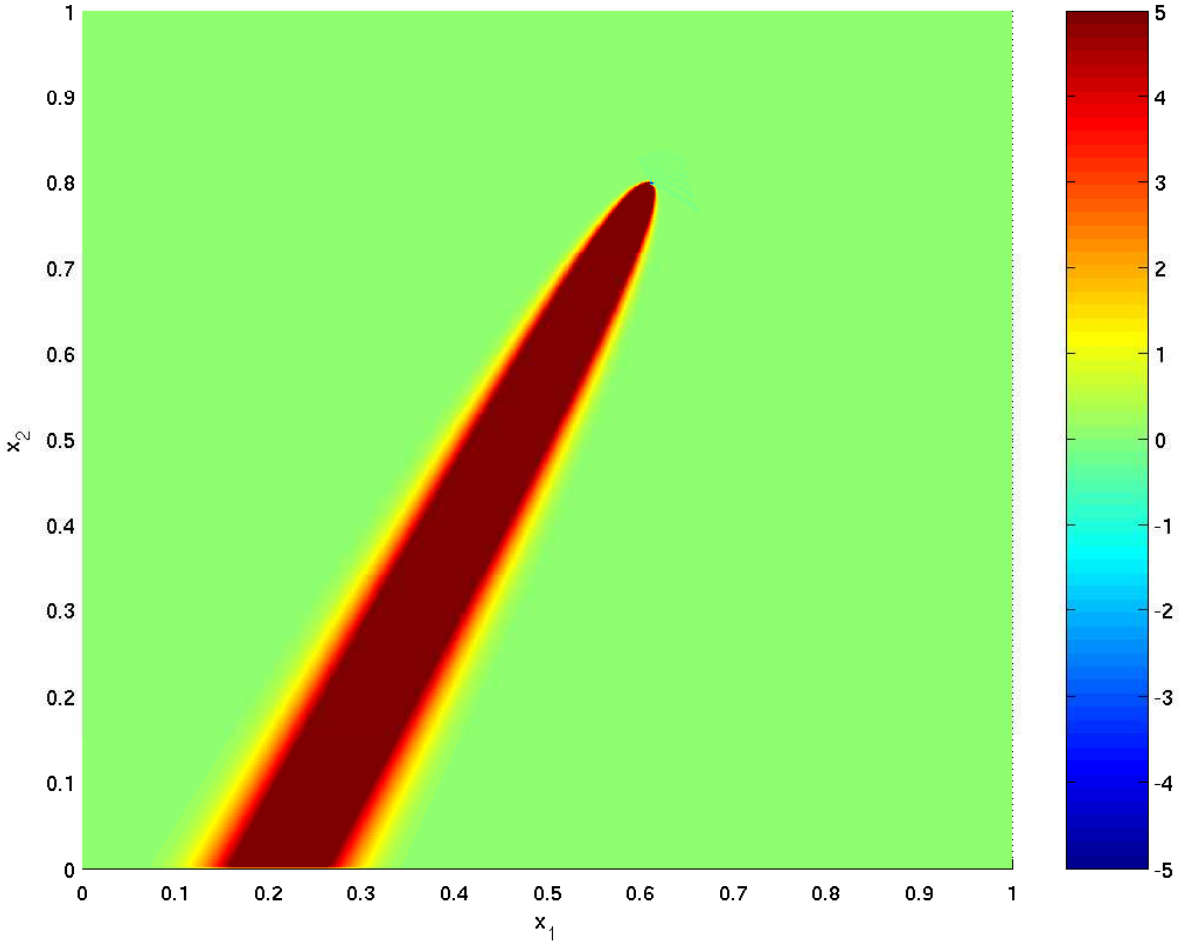

Figure 13: Contour plot of $x \mapsto g(x, y^*)$.

Let us return to the model problem (24), that is,

$$\mathcal{L}u = -\kappa\Delta u + \beta \cdot \nabla u = f \text{ in } \Omega, \qquad \text{with } u_{|\partial\Omega} = 0, \tag{52}$$

where κ and β are defined as above. We now consider a right-hand side f as defined in Figure 16.

The exact solution, shown in Figure 17, has an internal layer, due to the discontinuity of f, and boundary layers at $x_1 = 1$ and $x_2 = 1$.

We consider three meshes, shown in Figure 18 (note that the third mesh is the same as in Fig. 9). The three meshes are quite coarse for the problem considered. The coarse-scale approximations $\bar{u}$ are given in Figures 19–21 for $\mathcal{P}_{H_0^1}$ and $\mathcal{P}_{L^2}$. In Figure 19 it is very clear that the solution for $\mathcal{P}_{H_0^1}$ is much better than that for $\mathcal{P}_{L^2}$. In Figure 20, the solution for $\mathcal{P}_{H_0^1}$ is better than that for $\mathcal{P}_{L^2}$, but not by as wide margin as in Figure 19. The trend continues in Figure 21, but the solution for $\mathcal{P}_{H_0^1}$ is only slightly better than that for $\mathcal{P}_{L^2}$. We have tested other meshes, obtaining results

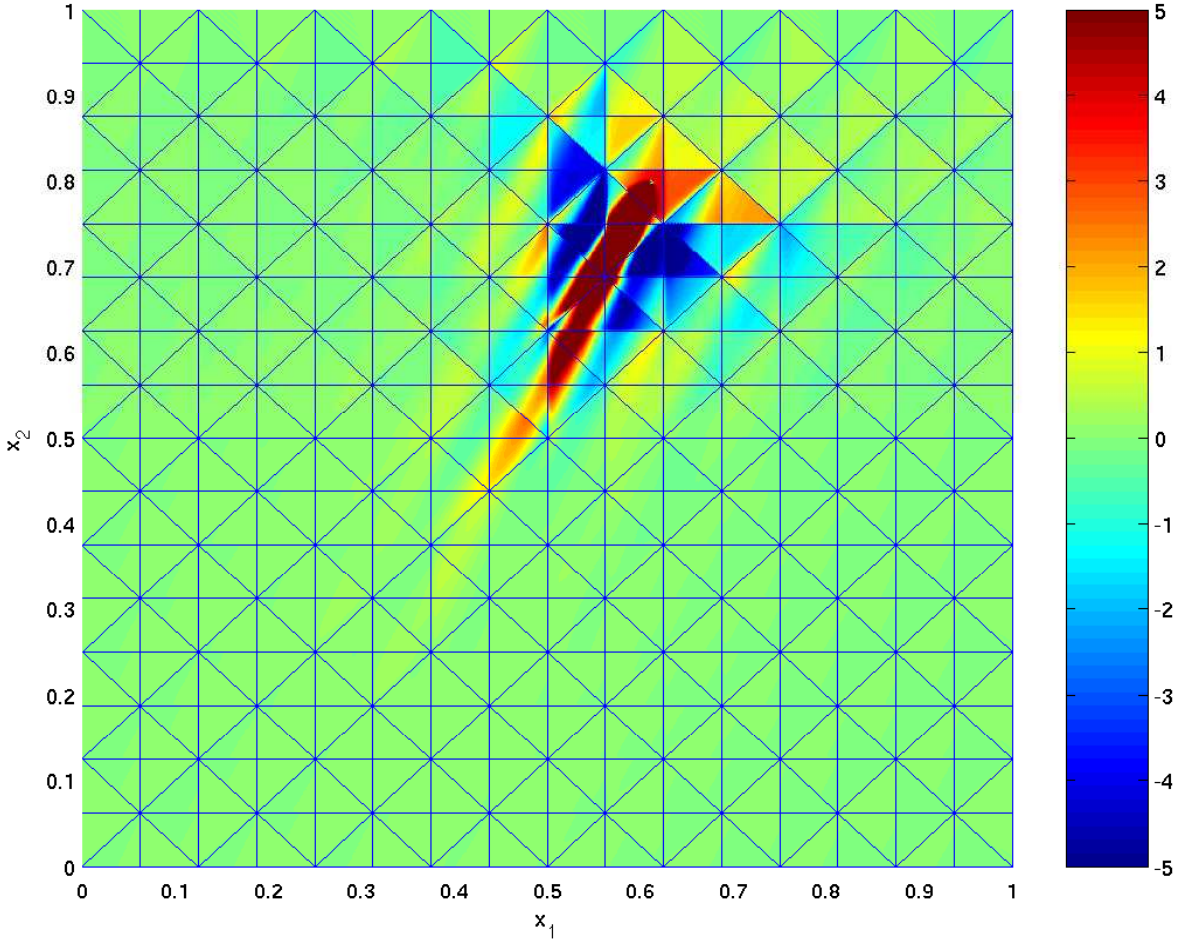

Figure 14: Contour plot of $x \mapsto g'(x, y^*)$ for $\mathcal{P} = \mathcal{P}_{H_0^1}$, and the associated coarse mesh.

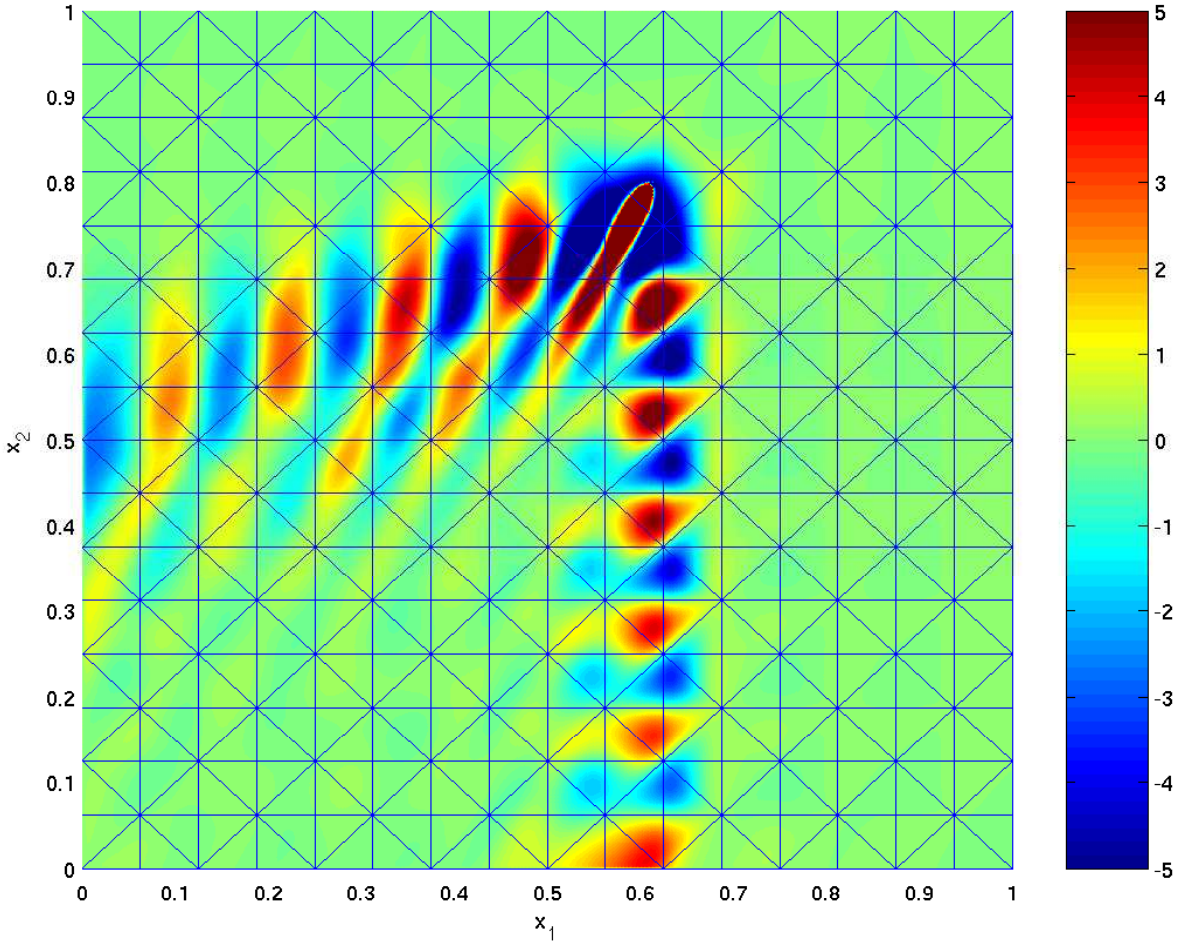

Figure 15: Contour plot of $x \mapsto g'(x, y^*)$ for $\mathcal{P} = \mathcal{P}_{L^2}$, and the associated coarse mesh.

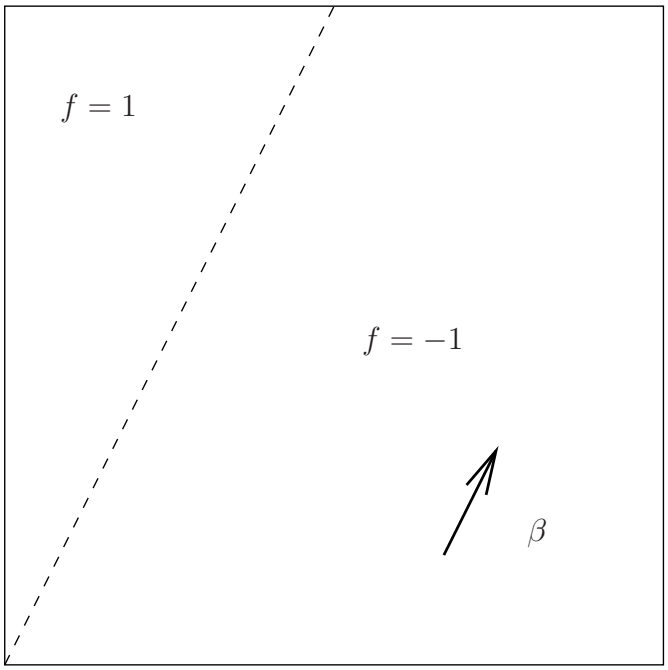

Figure 16: Right-hand side for the two-dimensional model problem.

(not shown) similar to the ones of Figure 19–21. The superiority of $\mathcal{P}_{H_0^1}$ seems to be a general fact, though it is more apparent for finer meshes than coarser meshes. One might conclude that H_0^1-optimality is not as strong condition than is often thought, and may not be enough in many practical cases for which monotonicity is deemed essential.

Remark 7. *In the present setting, one cannot ask for a nodally exact $\bar{u}$, because the functions of H_0^1 are not necessarily continuous. Formally, a g' for this purpose is given by (32), as for the one-dimensional case, but $g(x_i, x_i)$ is infinite, because g is singular.*

Remark 8. *In the case $\mathcal{P} = \mathcal{P}_{H_0^1}$, because of (29), we have, in the sense of distributions,*

$$\int_\Omega g'(x,y)\Delta\bar{v}(y)\,dy = 0, \qquad \forall \bar{v} \in \bar{V}.$$

Therefore, the fine-scale effect on the coarse-scale equation (30) becomes

$$\int_\Omega \int_\Omega \left(f(x) - \mathcal{L}\bar{u}(x)\right) g'(x,y)\mathcal{L}^*\bar{v}(y)\,dxdy = -\int_\Omega \int_\Omega \left(f(x) - \mathcal{L}\bar{u}(x)\right) g'(x,y)\beta\cdot\nabla\bar{v}(y)\,dxdy. \quad (53)$$

In one dimension, where g' is fully localized, the right-hand side of (53) is precisely the classical SUPG stabilization (see [9]), that is, the residual is weighted only by the advective part of the operator and the g' gives rise to the element-wise optimal τ, as described in Sections 3.1 and 3.2. (Recall that f was assumed to be a piecewise polynomial of degree at most $k-1$.) Note also that the diffusion operator in the residual in (53) may also be eliminated due to the aforementioned orthogonality property. These observations hold in higher dimensions as well, except g' is not fully localized within individual elements. In the classical multi-dimensional SUPG method [9], in place of (53), we have

$$-\sum_{e=1}^{n_{el}} \int_{\Omega_e} \left(f(x) - \mathcal{L}\bar{u}(x)\right) \tau(x)\,\beta\cdot\nabla\bar{v}(x)\,dx,$$

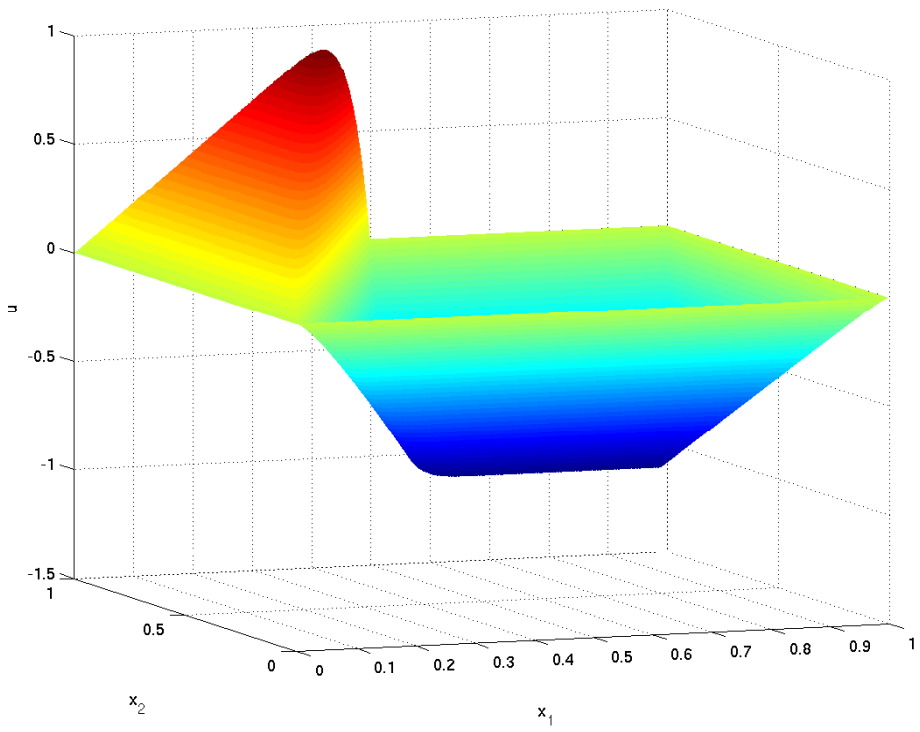

Figure 17: Exact solution u of the two-dimensional model problem.

where Ω_e, $e = 1, \ldots, n_{el}$, are the elements of the mesh on Ω. The primary difference between SUPG and (53) is that g' is replaced by the element-wise constant τ. This approximation may be justified in light of the localized nature of g'. Indeed, SUPG has been shown to converge at optimal rates in higher dimensions (see, for example, [18]), although, in advection-dominated cases, the "stability" norm is not as strong as the H_0^1-seminorm in that it only contains the streamline derivative.

Remark 9. *The residual-free bubble approach [4–8, 19, 20] has been shown in [3] to be equivalent to a multiscale method in which the fine-scale Green's function is approximated by a local, element Green's function [13, 14]. Use of a local Green's function, in light of the framework described herein, can only be rigorously justified in the one-dimensional case in which the H_0^1-projector is employed. However, this amounts to a very convenient approximation in practice, and one that is known to generate effective stabilized methods [1, 5, 6, 19]. With a better knowledge of g' in the multi-dimensional case, we would anticipate that improved stabilization schemes could be devised.*

4 Conclusions

In this paper we have derived an expression for the fine-scale Green's function arising in variational multiscale analysis. The specification of a projector, defining the direct-sum decomposition into coarse-scale and fine-scale components, renders the problem for the fine-scale Green's function well-posed. Different projectors give rise to different fine-scale Green's functions, and their properties can vary considerably. It is felt to be beneficial if the fine-scale Green's function is more attenuated than the classical Green's function and its support is dominantly local. It is found that the projector induced by the H_0^1-seminorm enjoys these properties whereas the projector induced by the L^2-norm does not.

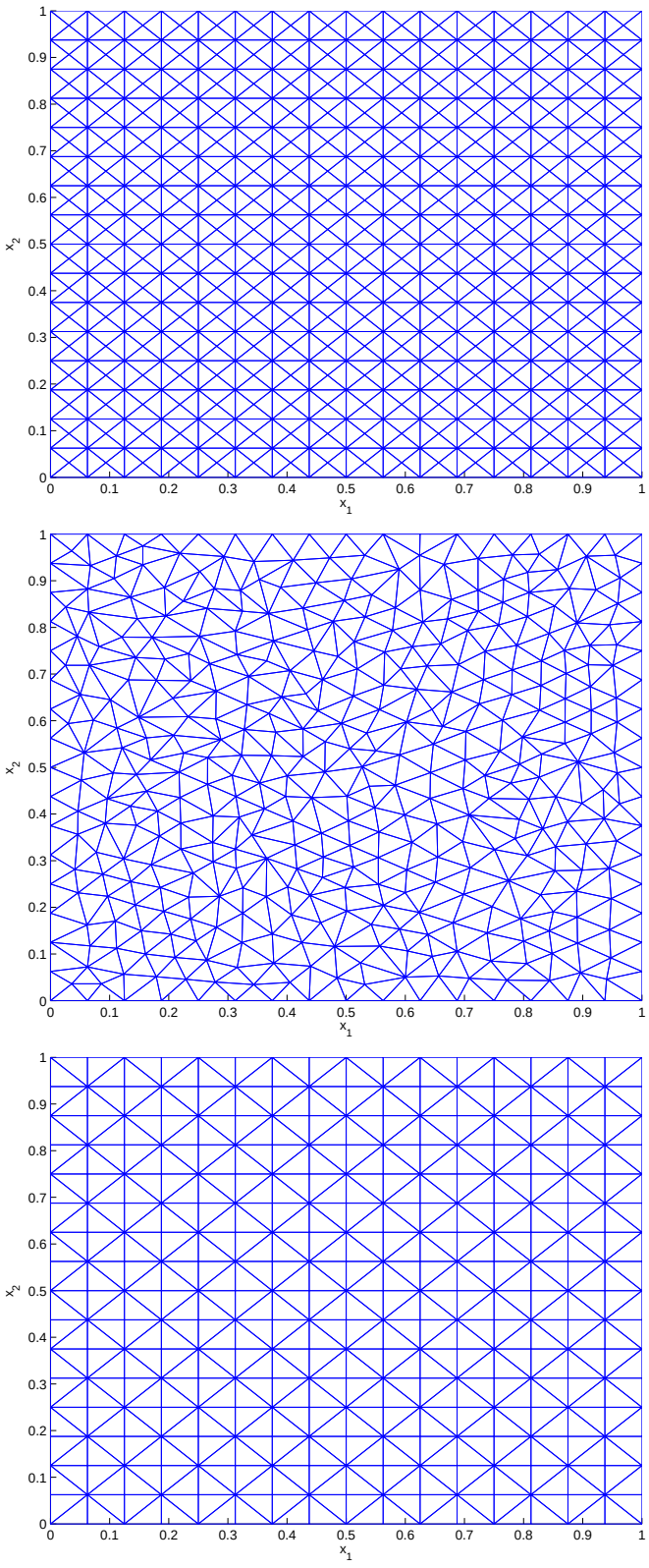

Figure 18: Meshes of the coarse-scale spaces $\bar{V}$ used for the calculations of the coarse-scale components $\bar{u}$ of the model problem (52).

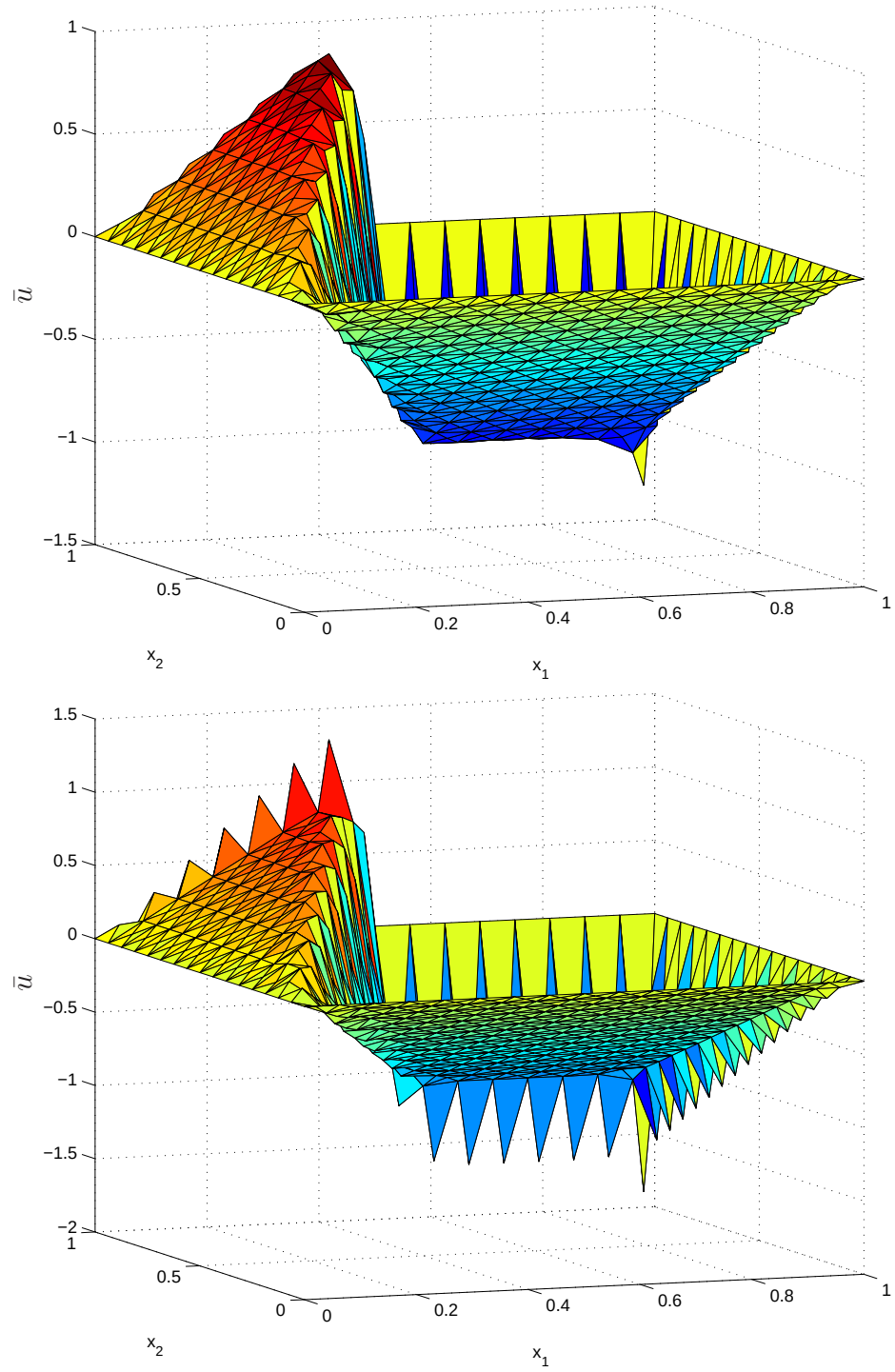

Figure 19: Coarse-scale component $\bar{u}$ for problem (52). $\mathcal{P} = \mathcal{P}_{H_0^1}$ (above) and $\mathcal{P} = \mathcal{P}_{L^2}$ (below). The coarse-scale space $\bar{V}$ is based on the first mesh of Figure 18.

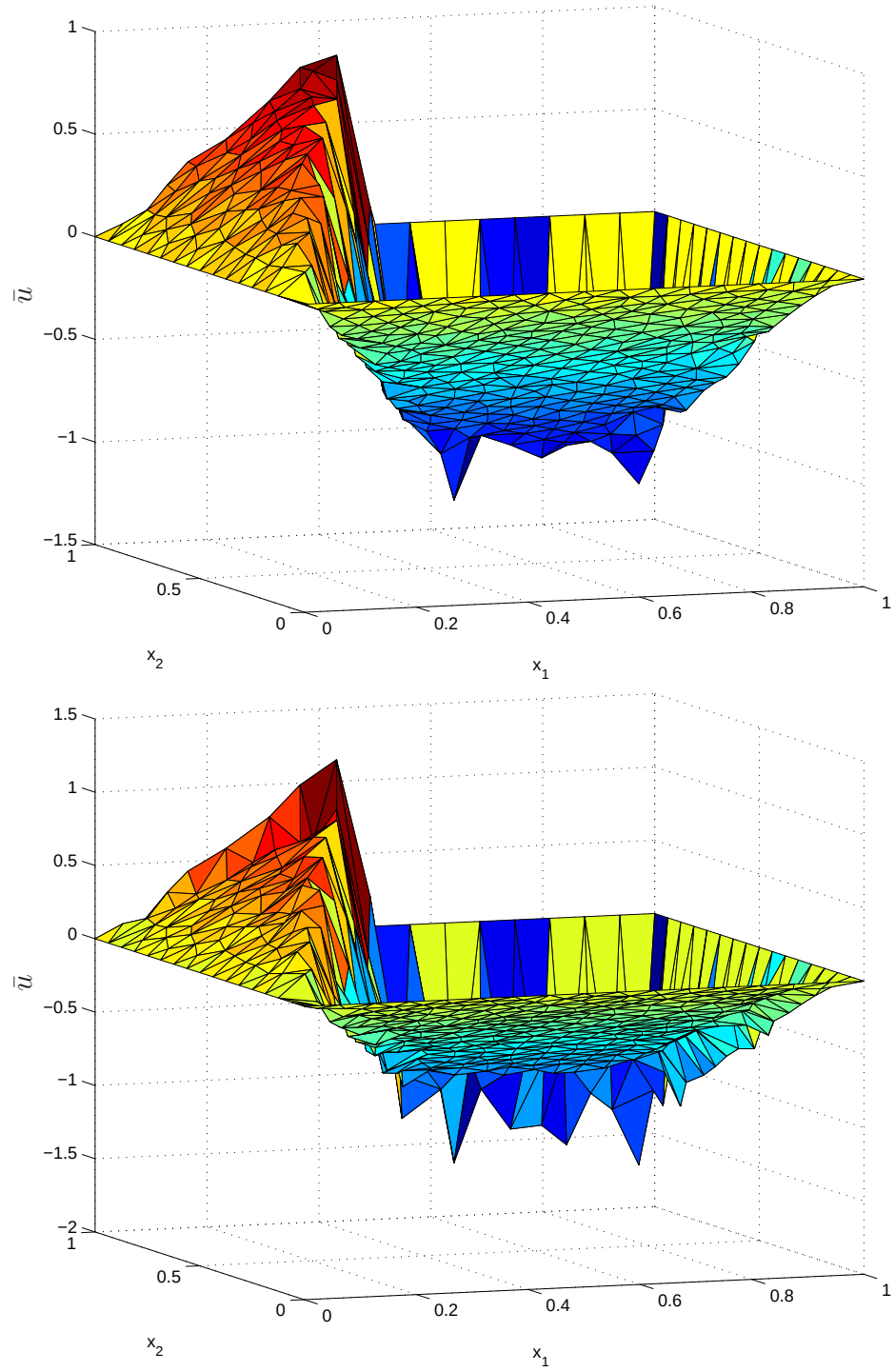

Figure 20: Coarse-scale component $\bar{u}$ for problem (52). $\mathcal{P} = \mathcal{P}_{H_0^1}$ (above) and $\mathcal{P} = \mathcal{P}_{L^2}$ (below). The coarse-scale space $\bar{V}$ is based on the second mesh of Figure 18.

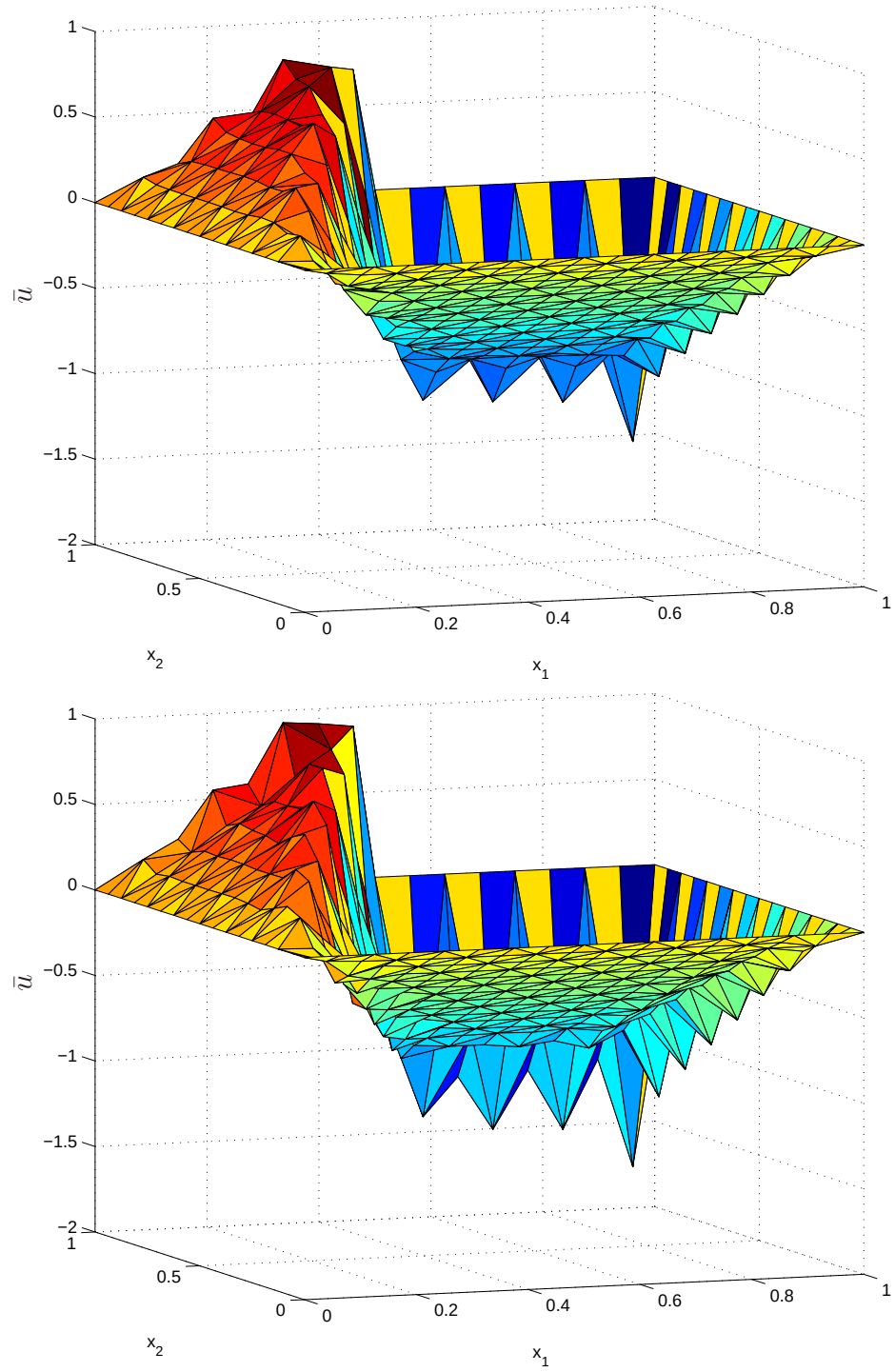

Figure 21: Coarse-scale component $\bar{u}$ for problem (52). $\mathcal{P} = \mathcal{P}_{H_0^1}$ (above) and $\mathcal{P} = \mathcal{P}_{L^2}$ (below). The coarse-scale space $\bar{V}$ is based on the third mesh of Figure 18.

The primary practical result of these studies is in the development of a framework for approximate multiscale methods. Indeed, in general it is not possible to exactly calculate the fine-scale Green's function. Despite its complexity, its orthogonality properties suggests simplified constructs in the form of stabilized methods. This is instantiated precisely in one dimension for the H_0^1-projector and its possibility in higher dimensions is suggested as well. In fact, it is shown that the H_0^1-optimal method and SUPG have features in common.

The results obtained clarify the relationship between the fine-scale Green's function and the properties of the coarse-scale solution. However, we only considered projectors associated with inner products and, in particular, we only studied the H_0^1- and L^2-projectors. The coarse-scale solution achieves optimality in terms of the corresponding norm. One could conceive of requiring the coarse-scale solution to achieve optimality in other measures giving rise to nonlinear structure. This is an intriguing possibility in that one could, for example, require monotonicity, or other desirable behavior. In the past, *ad hoc* procedures have been used to instill such properties in numerical methods, but the present ideas seem to have the potential for studying these issues in a more fundamental way.

Presently, most numerical methods are given as recipes and they are evaluated *ex post facto* by the way they satisfy desired objectives. The present developments suggest a different approach: designing numerical methods to satisfy desired objectives *ab initio*. We are a long way from making this a practical reality but we believe some small steps have been taken in this direction.

Acknowledgment

The work of T.J.R. Hughes was supported by Sandia Contract No. A0340.0 with the University of Texas and is gratefully acknowledged. G. Sangalli thanks the Institute for Computational Engineering and Sciences (UT-Austin) for kind hospitality and the financial support of the J. Tinsley Oden Faculty Fellowship Research Program. We thank Rich Lehoucq for insightful remarks and inspirations.

References

[1] M. I. Asensio, A. Russo, and G. Sangalli, *The residual-free bubble numerical method with quadratic elements*, Math. Models Methods Appl. Sci., 14 (2004), pp. 641–661.

[2] F. Brezzi and M. Fortin, *Mixed and hybrid finite element methods*, Springer-Verlag, New York, 1991.

[3] F. Brezzi, L. P. Franca, T. J. R. Hughes, and A. Russo, $b = \int g$, Comput. Methods Appl. Mech. Engrg., 145 (1997), pp. 329–339.

[4] F. Brezzi, L. P. Franca, and A. Russo, *Further considerations on residual-free bubbles for advective-diffusive equations*, Comput. Methods Appl. Mech. Engrg., 166 (1998), pp. 25–33.

[5] F. Brezzi, T. J. R. Hughes, L. D. Marini, A. Russo, and E. Süli, *A priori error analysis of residual-free bubbles for advection-diffusion problems*, SIAM J. Numer. Anal., 36 (1999), pp. 1933–1948.

[6] F. Brezzi, D. Marini, and E. Süli, *Residual-free bubbles for advection-diffusion problems: the general error analysis*, Numer. Math., 85 (2000), pp. 31–47.

[7] F. Brezzi and L. D. Marini, *Augmented spaces, two-level methods, and stabilizing subgrids*, Internat. J. Numer. Methods Fluids, 40 (2002), pp. 31–46. ICFD Conference on Numerical Methods for Fluid Dynamics (Oxford, 2001).

[8] F. Brezzi and A. Russo, *Choosing bubbles for advection-diffusion problems*, Math. Models Methods Appl. Sci., 4 (1994), pp. 571–587.

[9] A. N. Brooks and T. J. R. Hughes, *Streamline upwind/Petrov-Galerkin formulations for convection dominated flows with particular emphasis on the incompressible Navier-Stokes equations*, Comput. Methods Appl. Mech. Engrg., 32 (1982), pp. 199–259. FENOMECH '81, Part I (Stuttgart, 1981).

[10] L. P. Franca and E. G. Dutra do Carmo, *The Galerkin gradient least-squares method*, Comput. Methods Appl. Mech. Engrg., 74 (1989), pp. 41–54.

[11] J. Holmen, T. J. R. Hughes, A. A. Oberai, and G. N. Wells, *Sensitivity of the scale partition for variational multiscale large-eddy simulation of channel flow*, Physics of Fluids, 16 (2004), pp. 824–827.

[12] T. J. Hughes, L. Mazzei, and K. E. Jansen, *Large eddy simulation and the variational multiscale method*, Computing and Visualization in Science, 3 (2000), pp. 47–59.

[13] T. J. R. Hughes, *Multiscale phenomena: Green's functions, the Dirichlet-to-Neumann formulation, subgrid scale models, bubbles and the origins of stabilized methods*, Comput. Methods Appl. Mech. Engrg., 127 (1995), pp. 387–401.

[14] T. J. R. Hughes, G. R. Feijóo, L. Mazzei, and J.-B. Quincy, *The variational multiscale method—a paradigm for computational mechanics*, Comput. Methods Appl. Mech. Engrg., 166 (1998), pp. 3–24.

[15] T. J. R. Hughes, L. Mazzei, A. A. Oberai, and A. A. Wray, *The multiscale formulation of large eddy simulation: Decay of homogeneous isotropic turbulence*, Physics of Fluids, 13 (2001), pp. 505–512.

[16] T. J. R. Hughes, A. A. Oberai, and L. Mazzei, *Large eddy simulation of turbulent channel flows by the variational multiscale method*, Physics of Fluids, 13 (2001), pp. 1784–1799.

[17] T. J. R. Hughes, G. N. Wells, and A. A. Wray, *Energy transfers and spectral eddy viscosity in large-eddy simulations of homogeneous isotropic turbulence: Comparison of dynamic smagorinsky and multiscale models over a range of discretizations*, Physics of Fluids, 16 (2004), pp. 4044–4052.

[18] C. Johnson, U. Nävert, and J. Pitkäranta, *Finite element methods for linear hyperbolic problems*, Comput. Methods Appl. Mech. Engrg., 45 (1984), pp. 285–312.

[19] G. Sangalli, *Global and local error analysis for the residual-free bubbles method applied to advection-dominated problems*, SIAM J. Numer. Anal., 38 (2000), pp. 1496–1522.

[20] ——, *Capturing small scales in elliptic problems using a residual-free bubbles finite element method*, Multiscale Model. Simul., 1 (2003), pp. 485–503.

[21] I. Stakgold, *Green's functions and boundary value problems*, Pure and Applied Mathematics (New York), John Wiley & Sons Inc., New York, second ed., 1998. A Wiley-Interscience Publication.